Chemical Control of Graphene Architecture: Tailoring Shape and Properties

Raymond L. D. Whitby*

School of Engineering, Nazarbayev University, 53, Kabanbay Batyr Avenue, Astana 010000, Kazakhstan and Nanoscience & Nanotechnology Group, Huxley Building, University of Brighton, Brighton, Sussex BN2 4GJ, United Kingdom

ABSTRACT Single layer graphene and graphene oxide feature useful and occasionally unique properties by virtue of their two-dimensional structure. Given that there is a strong correlation between graphene architecture and its conductive, mechanical, chemical, and sorptive properties, which lead to useful technologies, the ability to systematically deform graphene into three-dimensional structures, therefore, provides a controllable, scalable route toward tailoring such properties in the final system. However, the advent of chemical methods to control graphene architecture is still coming to fruition and requires focused attention. The flexibility of the graphene system and the direct and indirect methods available to induce morphology changes of graphene sheets are first discussed in this review. Focus is then given toward chemical reactions that influence the shape of presynthesized graphene and graphene oxide sheets, from which a toolbox can be extrapolated and used in controlling the spatial arrangement of graphene sheets within composite materials and ultimately tailoring graphene-based device performance. Finally, the properties of three-dimensionally controlled graphene-based systems are highlighted for their use as batteries, strengthening additives, gas or liquid sorbents, chemical reactor platforms, and supercapacitors.

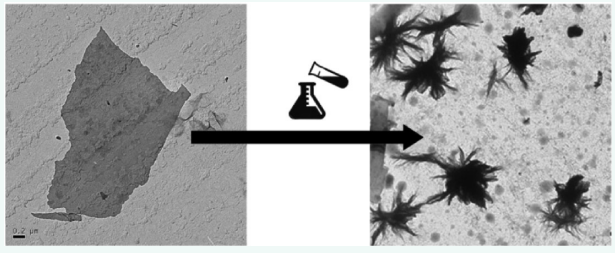

KEYWORDS: graphene · graphene oxide · chemistry · architecture · properties · electronics · energy storage · sorption · mechanical reinforcement

Structure and Properties of Planar Graphene. Graphene is typically defined as a single layer of sp^2 carbon atoms arranged in a sheet and in a rudimentary form can be visualized to be a single exfoliated layer from graphite (Figure 1). The layering in graphite is separated by 3.4 Å in highly crystalline $P6_3/mmc$ crystal and allows slippage between the layers, under standard conditions. The ability of graphite layers to slide due to weaker van der Waals forces, as compared with covalent forces, ultimately allowed the shearing of graphite and isolation and imaging of the first single-layer graphenes.[1] When the individual sheet was separated from its supporting neighbors, or single and double sheets were prepared on metallic surfaces, the anomalous quantum Hall effect was determined, which is not readily evident when the number of layers $n > 2$, or when there is strong interaction between the graphene layer and the support substrate.[2]

Graphene typically refers to a monolayer of carbon atoms packed into a honeycomb crystal structure, which are one-atom thick of sp^2 bonded carbon, thus yielding a two-dimensional array of carbon arranged in a hexagonal structure (Figure 2). The carbon−carbon bond length in graphene is 1.42 Å, verified with high resolution electron microscopy, atomic force microscopy and scanning tunneling microscopy,[4] which comprise σ orbitals binding with their neighbors and yield the strength and flexibility of the lattice. While the simplified structure of graphene is that of a flat sheet (Figure 1a), the observed structure is often corrugated (Figure 1b). The rippling effect of graphene has been determined to be in part due to stabilization due to thermal fluctuations across the sheet when suspended in air or a vacuum.[3,5,6] The undulating structure of graphene, which therefore represents entry into 3 dimensions, has also been

* Address correspondence to raymond.whitby@nu.edu.kz, r.whitby@brighton.ac.uk.

Received for review August 14, 2014 and accepted September 22, 2014.

Published online September 22, 2014
10.1021/nn504544h

determined for graphene sheets in water. The extent of corrugation can be controlled, which was demonstrated useful for controlling the filtration of nanoparticle colloids through membranes of chemically altered graphenes and has the potential to prevent restacking of graphene into graphite and instead control the assembly of three-dimensional matrices where the high surface area of graphene is retained for applications such as energy storage.[7]

The revolution to the carbon world in the form of nanosized carbon, above and beyond that of fullerenes, carbon nanotubes, nanohorns, nanodiamonds, *etc.*, cannot be understated and in the interest that ensued it has become important to further classify the graphene in terms of the number of layers. Numerous reports are published containing the label "graphene", yet contain several layers arranged in a manner that is typically associated with the graphite lattice. The mechanical processing of graphite, expanded graphite and exfoliated graphite typically generate platelets with more than 20 layers. When comparing such systems to those with *n* from 2 to 20, differences in flexibility can be observed through wrinkling and folding of the fewer number of graphene layered systems. It is unclear under what conditions the "multilayer graphene" label can be applied, though discussion may extend to the degree of physical separation of the layers, namely the difference between expanded graphite and stacked single-layer graphene. To that end, chemical bridging has been used to generate porous graphene oxide frameworks where the graphene sheets are maintained in an open, stacked conformation, which has been useful for gas sorption[8,9] and chemical catalysis.[10] In this review, graphene is referred to as a single layer system, unless stated otherwise, and the context differentiates between the nonoxidized and oxidized forms.

Graphene has a Young's modulus of *ca.* 1 TPa and an intrinsic strength of *ca.* 130 GPa.[11] Graphene oxide has a lower Young's modulus of *ca.* 210 GPa and intrinsic strength of *ca.* 75 MPa.[12] Pure graphene is zero-bandgap semiconductor and possesses an electron mobility of 15 000 $cm^2/(V \cdot s)$ at room temperature,

VOCABULARY: graphene architecture – the 3-dimensional shape of an individual graphene sheet or its spatial arrangement within a given system; **3-dimensional template** – a substrate, either sacrificial or permanent, that supports the deposition of a material in 3 dimensions; **intra/intersheet bonding** – the chemical bonding of graphene between two sites on the same sheet and between two sites on different sheets respectively; **hierarchical ordering** – the arrangement of individual graphene sheets that has different levels of architecture between the nano- and macro-scale; **graphene sheet chemistry** – the process of chemical transformation directly on the graphene lattice or through other chemical groups attached to the graphene lattice;

with ballistic electron transport.[13] The individual graphene sheet has a theoretical specific surface area of 2630 $m^2 \cdot g^{-1}$,[14] which is substantially higher than that of graphite. These properties make graphene an attractive material in electronics and building applications and the flexibility, along with high surface area, of the graphene sheet has also promised designer adsorbents and drug delivery capabilities, which has led to the direct manipulation of graphene architecture in 3 dimensions.[15]

The interface between the substrate and a graphene layer can result in discrete areas of chemisorption interaction, as determined by low energy electron diffraction patterns and DFT calculations between the two, and can affect the morphology and electronic properties of graphene. Rippling was found to occur in

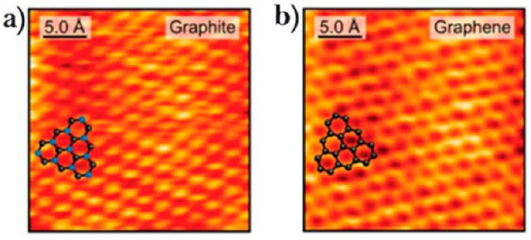

Figure 2. Scanning tunneling microscopy images of (a) a graphite and (b) a graphene structure. Reprinted from ref 4. Copyright 2010 American Chemical Society.

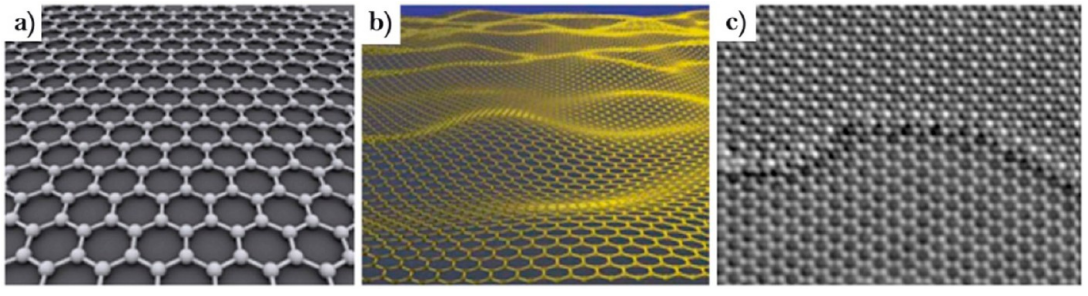

Figure 1. Computer models of graphene revealing (a) the hexagonal lattice of carbon atoms for ming a "true" planar layer and (b) the undulating nature of graphene exhibited by real samples. (c) An exit wave function reconstruction in TEM mode of graphene revealing a single and bilayer where the honeycomb structure of carbon atoms is evident. Reprinted with permission from ref 3. Copyright 2007 Nature Publishing Group.

graphene when interfaced with iridium and heated to *ca.* 500 °C yielding a buckling height of 2.1 Å, where thermal effects exert different degrees of expansion between the graphene sheet and the substrate creating strain that is relieved through corrugation. The corrugation is reversible, where the graphene sheet can be changed between flat and buckled conformations with respect to the underlying substrate. The strong interaction between the substrate and the graphene layer alters the Dirac cones, leading to nonzero density of states of the buckled areas, which were deemed not linked to the buckling architecture but the chemisorption interface. Ultimately, the system changes the electronic property of graphene from a semimetallic to a metallic state, only as a result from the small fraction of atoms considered to be chemisorbed at the Ir−C interface,[16] with the majority of the graphene remaining physisorbed to the iridium surface. When the number of graphene layers is increased, the perturbation of the electronic structure near the Fermi level diminishes until the system behaves as free-standing graphene.[17]

The presence of pristine graphene sheets within nonconductive matrices can reduce the electrical resistivity of the host. Therein, the graphene sheets become conductive pathways within electrically insulating polymers. Thermally expanded graphite oxide at 1000 °C under argon leads to functionalized graphene,[18] but can also reduce single layer graphene oxide (SLGO) to single layer graphene (SLG).[19] Reduction can improve electrical conductivity by removal of oxygen containing groups and restoration of the aromatic nature of bonding, establishing the delocalization of π-electrons across the surface of the graphene sheet, frequently appearing wrinkled in morphology (Figure 3a). The electrical conductivity of SLGO (cast as buckypaper)[20] is on the order of 8.5×10^{-2} S/cm and thermally reduced SLGO in argon, to produce graphene, is 8.1×10^{3} S/cm.[19] When graphene sheets are placed in nonconductive polymers, such as polyvinylidene fluoride (PVDF), the sheet size, aspect ratio, and morphology aid the sheet−sheet interconnectivity, providing conductive pathways through regions of nonconductive polymer particles (Figure 3b).[21] It should be noted that the filler does not need to be in direct contact for current flow. Conduction may take place through tunneling between layers of polymer that borders the filler material, which if thin enough provide (a quantum mechanical probability of) tunneling through the resistance barrier.[22] It was determined that the sheet area affected electrical conductivity more strongly than sheet density.[23] In graphene−PVDF composites, the percolation threshold was around 2 wt %, compared with expanded graphite−PVDF composites where the percolation threshold was around 5 wt %.[21] The lower filler loading was attributed to a higher aspect ratio of graphene to that of expanded graphite. It has also been

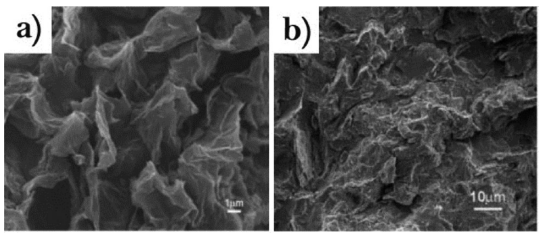

Figure 3. SEM images of (a) thermally expanded and reduced graphite oxide leading to conductive graphene sheets in a wrinkled morphology and (b) random distribution of thermally reduced graphene sheets in polyvinylidene fluoride, where the wrinkled morphology is retained. Reprinted with permission from ref 21. Copyright 2009 Wiley-VCH Verlag GmbH.

recently found that very low loadings (*ca.* 0.045 vol %) of graphenes in poly(*N*-isopropylacrylamide) generate superelastic graphene aerogels that exhibit high electrical conductivity and good mechanical strength without sacrificing stimuli-responsiveness of the polymer. Therein, the conductivity reached 0.7 $S \cdot m^{-1}$ for *ca.* 0.045 vol % and 10 $S \cdot m^{-1}$ with *ca.* 0.23 vol % graphene loading, higher than other hierarchical systems using reduced graphene oxide-based hydrogels at similar loading levels.[24]

In one-dimensional nanomaterial systems, such as carbon nanotubes, percolation was affected by alignment of the nanomaterial filler. Optimal orientation of carbon nanotubes was found when they were partially aligned rather than randomly or perfectly aligned.[25] In two-dimensional systems, electrical conductivity is highly sensitive to the morphology of the nanomaterials along the percolation pathway[26] and alignment of graphene sheets results in a lower number of electrical connections and fewer sheet−sheet contact points required to establish a conductive pathway.[27] It may be that wrinkling of graphene sheets leading to the generation of a series of fold lines, which may enhance electrically conductive properties,[28] therefore an optimized system would contain an arrangement of wrinkled graphene sheets that bring fold lines into alignment.

While the electrical conductivity of graphene−polymer composites can be improved, the significance of graphene architecture in polymers as reinforcing fillers has yet to be fully demonstrated. However, indications show that graphene's three-dimensional arrangement can influence the mechanical performance of polymer composites. Graphene oxide can hydrogen bond with poly(propylene carbonate) and become crumpled in solvent-exchange, solution casting of composites (Figure 4).[29] The extent of this crumpling becomes more pronounced as the content of graphene oxide is increased, which is thought also to be linked to the different stiffness between the polymer matrix and the graphene oxide sheets. As the loading of graphene oxide increases up to 10 wt %, the sheets form a network

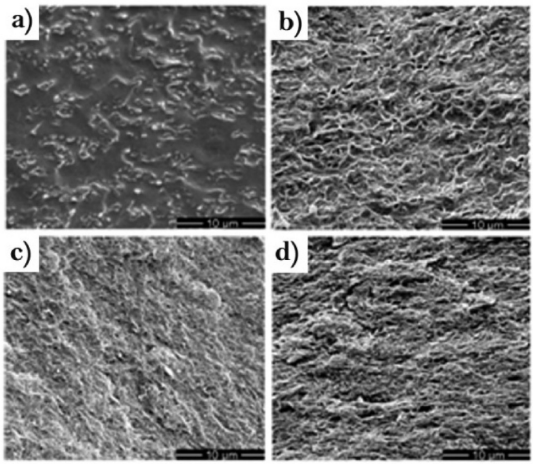

Figure 4. SEM images of GO in poly(propylene carbonate) at (a) 1, (b) 5, (c) 10, and (d) 20 wt %. Reprinted with permission from ref 29. Copyright 2014 IOP Publishing.

structure and the tensile strength increases to 33 MPa, and the Young's modulus increases to 4100 MPa at 20 °C and 6 and 250 MPa, respectively, at 75 °C. Between 10 and 20 wt %, graphene oxide sheets form a "co-continuous" arrangement,[30] and the tensile strength and Young's modulus change to 28 and 5500 MPa, respectively, at 20 °C and 3 and 370 MPa at 75 °C.[29] The graphene co-continuous architecture confines poly(propylene carbonate) chain movement and enables effect transfer of stress, thus improving mechanical properties.

Tailoring of materials ensures customized fit for its desired end use in terms of size, shape and properties and the ability of a system to adapt these aspects, as a result of environmental or operator input, will facilitate greater usability. Flexible electronics, for example, offer a wide-variety of applications including displays, batteries, solar cells, supercapacitors, and medical devices, and it is in these areas for which graphenes show significant promise.[14,31] Therefore, extending the tailoring of graphene's three-dimensional structure, especially where properties of the system result from the architectural configuration of its components, will result in maximum gains in the overall properties. Currently, there is a vast amount of data published for chemical reactions of graphenes, which occasionally demonstrate change from a two- to a three-dimensional structure; however, such changes, as influenced by a chemical reaction, are often a secondary consideration rather than primary focus. This work will detail the extent to which chemistry can be utilized to alter the graphene structure, whether through direct or indirect processes, but it is important to first cover graphene synthesis and its chemical environment.

Graphene Synthesis. There are many articles and review papers that deal with the synthesis of graphenes and graphene oxides,[14,32−37] but a brief recap is warranted given that the size, purity and shape of the individual graphene layers will determine their properties and can potentially impact the degree to which architectural changes may be conducted. Mechanical separation of graphite into SLG sheets generally results in high purity systems with dimensions in the order of a few micrometers.[1] Their high quality allows direct assessment of the fundamental properties of SLG revealing high thermal conductivity,[38] Young's modulus,[11] and electrical conductivity.[39] By itself, mechanical separation generates both SLG and multilayer graphene (MLG). Further separation has been attempted through surfactant-assisted disagglomeration.[40] The difficulty therein is the increase in likelihood of residual chemicals or through heating leading to carbonaceous material on the SLG surface. The major drawback with this approach has been the low quantities of SLG produced. It is understandable that without the assistance of surfactant dispersants the graphene sheets restack into a graphite structure.[40] However, the "temporary" exfoliation of graphene sheets and attempted restacking toward graphite-like structure have been useful for trapping nanomaterials to form intercalated composite structures. The control of their interlayer spacing will lead to application in supercapacitors that combine high energy density, high power density, and high operation rates.[41−43]

Alternative production strategies include the generation of graphenes on metal or metal carbide surfaces. Epitaxial growth of graphene relies on the weak interaction between the growing layer and supporting substrate. Multilayer graphene grown on SiC shows electronic properties similar to that of a single layer of graphene, where massless Dirac Fermions are detected; thus, there is no influence from the underlying support, although this is not always the case and interlayer screening effects can result within multilayer graphene systems on SiC.[44] Silicon carbide can be reduced to generate 1 or more layers of graphene, which are dependent on the original size of the SiC wafer, thus providing control over the final size of the graphene. Removal of graphene from this system is not an easy endeavor and does not lend itself to bulk scale synthesis of high quality graphene.

It is possible to produce graphenes on metal substrates, but there are limitations depending on the type of metal used. Ruthenium can support the growth of graphene, but often lacks uniformity in its thickness. There is also interaction between the metal substrate and graphene interface, which can affect its properties. However, the metal substrate can be removed through dissolution in order to leave a free graphene layer and therefore provides a route toward scalable production. Copper substrates have been used successfully in the generation of graphene, where the growth of graphene self-terminates after the first layer. The system is also dependent on the type of carbon feedstock

used. The use of iridium as a support growth platform is relevant to this discussion. It provides a sufficiently weak interaction with the graphene grown and the thickness of the graphene layer is uniform over a large surface area of the iridium substrate. Therein, the geometry of graphene is not exactly planar, but slightly rippled, which contributes toward gaps in the electronic band structure[45] and indicates the important link between the graphene architecture and its properties.

Other approaches toward SLG focus on strategies to exfoliate graphite in liquid media, using solvent or surfactant to assist separation into SLG. To obtain high quantities of high purity SLG, the feedstock becomes very important. As with mechanical exfoliation, the starting graphite must be of high purity to ensure the separated layers are too. However, an ideal starting material would be graphite-like with a greater interlayer separation to facilitate exfoliation of single layers. Investigations are proceeding toward intercalation of graphite with liquid phases,[46−48] chemical[49,50] or surfactants[51] and design of thermally expanded (carbonizable) polymers,[52,53] where the structure of the individual graphene layers remains intact, but in an expanded form to aid the exfoliation stage.

Graphene Oxide Synthesis and Chemical Environment. While there are many possible routes toward graphene production, the current widely accepted avenue is the use of the modified Hummers' method to generate graphene oxide,[54] conduct a reduction in order to remove any oxygen groups and generate properties as featured with pure graphene. Graphene oxide is therefore produced from the oxidation and subsequent exfoliation of graphite. Herein, oxidizing acids can intercalate the graphite structure, which does not always change the interlayer spacing, but through the oxidation of the carbon layers introduces defects and oxygen groups. It is the generation of the latter that causes the interlayer spacing to increase,[55] combined with the surface charge,[56] which can be exploited through sonication in order to separate individual layers of graphene as SLGO, along with other graphene and graphite oxide products. These can be separated through centrifugation and size separation techniques in order to increase product purity. After formation, it is then possible to chemically[56−58] or thermally reduce[59,60] the oxygen containing groups in order to produce SLG or more precisely reduced SLG (SLGR). These graphene systems may retain a number of oxygen groups and lattice defects;[57,61] however, their properties are often comparable to pure SLG systems.[62] This gives a useful route toward manipulation of the graphene surface chemistry to enable dispersion of conductive graphene systems without the need for surfactants. Therefore, three-dimensional composites as a sandwich structure can be assembled through the repetitive immersion of a substrate into negatively charged graphene-dispersed colloid solution and a positively charged polycation solution.[56] The ability to produce stable graphene solutions enables greater control over chemically assisted assembly of graphene-based devices as low-cost solution processing techniques.[40]

The chemical environment of graphene oxide has also been used to disperse other hydrophobic carbon nanomaterials, such as pristine single-walled carbon nanotubes, into water. Herein, attractive interaction of unfunctionalized regions of graphene oxide and the carbon nanotube enables effective coupling of the two systems, which achieves stability in aqueous solution through the oxygen-containing groups, providing electrostatic repulsive charges.[63]

It is worth briefly considering the purity and chemistry of graphene oxide systems, as they are advantageous in the control of graphene-based architecture. The generation of oxygen groups on graphene is well-inferred from previous studies on graphite oxide, in particular thin lamella of graphite oxide, which in today's definitions may be equally well referred to as multilayered graphene oxide.

The oxidation of a carbon system is known to lead to etching of the graphite lattice and the generation of oxygen-containing functional groups. A secondary effect is that the process also leads to functionalization of carbonaceous material as well as incomplete destruction of the graphene lattice, resulting in the presence of small, highly functionalized polycyclic aromatic hydrocarbons[64] known as fulvic acids,[65] carboxylated carbonaceous fragments,[66] or oxidation debris.[67] In acidic media, these become hydrophobic and immobilize on the surface of carbon materials, which is prevalent in many carbon systems undergoing acid oxidation. In turn, their presence and their chemistry can directly affect the carbon system. In one study, the presence of fulvic acids accounted for 17−24% of the mass of (modified Hummers' method produced) graphene oxide, and once removed from the surface, the remaining SLGO sedimented from solution indicating that a significant portion of the oxygen groups resided on the fulvic acids, which enhances the stability of the SLGO in solution.[68] The removal of fulvic acids also resulted in greater electrical conductivity, suggesting that these fulvic acids act as insulators coating the graphene surface. However, the presence of fulvic acids on SLGO is not always detected, where the purification strategy of SLGO failed to indicate any detachable carbon fragments.[61] It is therefore surmised that the graphite starting material, plus minor differences in the chemistry and processing, lead to variations in the final product; no two SLGO samples or even SLGO sheets are identical. In addition to increasing electrical resistance, the presence of fulvic acids on carbon nanomaterial surfaces also can lower the mechanical strength of carbon nanomaterial−polymer composites, due to the weaker interfacial forces between the fulvic acid and the carbon nanomaterials

surface, when compared with a purely covalent carbon nanomaterial-polymer composite system.[69]

Once the fulvic acids are removed, purified SLGO layers are left with oxygen-groups covalently bonded to the graphene lattice, distributed at the periphery and across the upper and lower surfaces. Studies indicate that the type and distribution of oxygen groups on graphene match the Lerf-Klinowski model.[70,71] All the major types of oxygen groups are represented in the analysis of graphene oxide, which comprise of carboxylic, lactone, phenol, anhydride, carbonyl, tertiary hydroxyl and ether.[33,61] Additional insight has been garnered from solid-state NMR analysis of graphite oxide where five- and six-membered-ring lactols were elucidated, but currently inferred with reasonable expectation that they exist in SLGOs. The distribution and quantity of these groups vary between studies, thus reinforcing the idea that no two SLGO systems are identical. But the availability of such groups also proffers access to a realm of chemistry to modify the structure, functionality and properties of graphene.[14,33]

Folding, Scrolling, and Bending of Graphene Sheets. The chemical properties on the surface of graphene are crucially important when interacting with other entities, especially liquids for stabilization of graphene suspensions, which are useful for processing.[72] Graphene interaction with materials, including neighboring graphene sheets or itself through a fold event, brings about a complex array of interactions, where surface forces become a predominating influence when the system is reduced to the nanoscale. $\pi-\pi$ bond interactions between the graphene sheet and polycyclic aromatic hydrocarbons account for the surface immobilization of graphite-derived and graphene lattice-derived fulvic acids under acidic conditions.[68] In the presence of graphene oxide, the oxygen-containing groups facilitate hydrogen bonding and electrostatic attractions with chemicals system, which has been used in the cross-linking of graphene oxide prior to hydrothermal treatment in order to generate a three-dimensional porous network capable of releasing the molecule acting as a cross-linking agent.[73]

Van der Waals attractive forces dominate the graphene surface and for SLG give an adhesion energy of *ca.* 0.45 J/m^2, similar to solid−liquid interaction, whereas 2−5 layers of graphene have an adhesion energy of 0.31 J/m^2. It was determined that the high adhesion energy allows the graphene sheet to conform to a variety of surfaces, which is useful for manipulating graphene around two- and three-dimensional templates.[74] In a fold event, where the graphene overlaps itself, the two areas of the graphene sheet interact and adhere, but this operates at the expense of deformation to the graphene lattice at the bend site. The deformation induces lattice strain and acts as a restoring force, trying to bring the graphene sheet back to a planar (or near planar) configuration. However, when the attractive forces in the sheet overlap region are greater than the restoring force at the bend site, the graphene sheet will bend and can be stably held in the folded conformation.[75]

The interplay of forces at the graphene surface will affect and be affected by the chemistry and processing conditions of graphene-based reactions leading to deformation and stabilization of graphene, often with three-dimensional architecture. It has been shown that graphene and graphene oxide can fold due to a variety of external stimuli, including thermal induction,[76] stress applied to the graphene sheet edges or externally applied loading across the whole sheet,[77,78] solvent evaporation from the graphene surface,[79] or freeze-drying.[80] When considering thermal fluctuations in the graphene system, the defining factors are linked to the size, aspect ratio and functionality of the graphene system as well as the external environment in which the graphene resides, where graphene ribbons (high in-plane aspect ratio) self-fold into scrolls and graphene sheets (low in-plane aspect ratio) maintain their planar state, depending on the temperature of the system. When considering application of stress to the graphene system, the aspect ratio is similarly important. The higher the aspect ratio, the greater the system deforms away from the planar structure of graphene, such that nanoribbons can be "seeded" with stress along the edge of the sheet, which leads to scrolling.[77] The ability to dope or functionalize the edge generates architectural changes whereby the electronic or magnetic properties of the graphene system are controlled.[81]

Highly contorted graphene structures, termed grafolds,[28] can form from the mechanical exfoliation process,[3] patterned substrates,[28] direct heating,[82] mechanical stimulation[75,83] or relaxation of strain during the cool down phase of graphene synthesis.[84] The simplest formation is folding into bilayer edges (Figure 5a),[85] which may exhibit unique electronic properties for device applications over that of stacked, nonfolded graphene layers.[86,87] When folding graphene, the lattice experiences stress at the site of curvature as well as interfacial (attractive and repulsive) forces between the areas of the folding layers that are brought into close proximity. These structures are stabilized through plane−plane interactions ($\pi-\pi$ interactions or attractive van der Waals forces) and the elimination of free edges,[85] but it is apparent that the graphene may have a preferential folding direction or location of the fold line, where graphene sheets tend to fold along armchair and zigzag directions.[83] Patterned copper foil have been used to exert folds within the graphene structure either through growth or transfer of planar graphene to the patterned substrate (Figure 5b).[28] Therein, a double folded (nonintercalated) graphene sheet reveals a semimetallic state with a minor indirect overlap between the occupied and unoccupied states,

running along the length of the fold.[28] The ability to control the location of folds within graphene will further enhance its electronic properties with the capacity to intercalate chemicals and materials within the layer at the fold site. Furthermore, the folding edge will be under higher lattice strain than a planar region of graphene and experience higher chemical reactivity, akin to curvature sites on carbon nanotubes.[88]

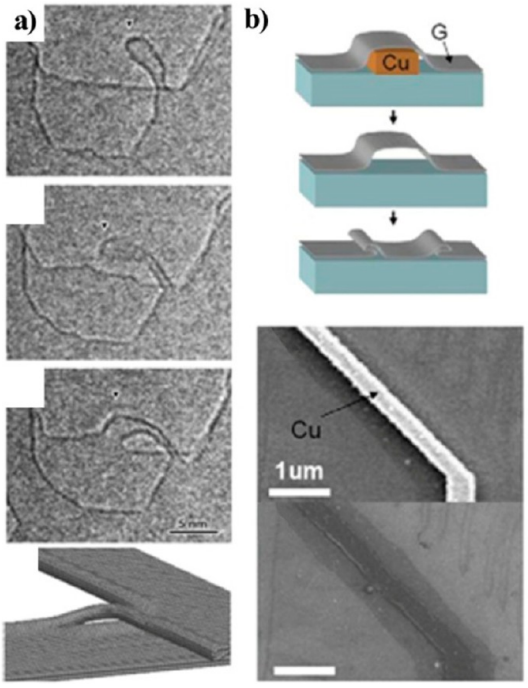

Figure 5. (a) *In situ* formation of carbon nanostructures, including graphene bilayer edges and carbon nanotubes resulting from heating graphene. (b) The synthesis of graphene on top of a profiled copper ridge induces a double pleat within the graphene layer after the removal of the copper support. Reprinted with permission from refs 85 and 28. Copyright 2009 National Academy of Sciences and 2011 American Physical Society.

When folding events occur, two areas of a graphene sheet come into close proximity and the graphene system must overcome the repulsive forces experienced between this new layer−layer interaction and layer-media (whether solvent or gas) interaction in order to stabilize the fold through attractive forces, the lattice strain at the bend site notwithstanding. This can be done by evaporating solvent from the surface of the graphene,[89] lowering the surface energy through the introduction of surfactants[90] or applying an electrostatic field.[91] The strength of the force exerted on a carbon surface can be readily seen through the deformation of carbon nanotube forests, from aligned carbon nanotube arrays, where evaporation of the solvent exerts surface tension on the carbon nanotubes toward common focal points[92] or through changing of the solvent where the density of carbon nanotube packing changes according to the surface tension of the liquid media used.[93]

In the case of graphene, surface tension forces exerted on the graphene layer during drying can lead to scrolling of the planar layer (Figure 6). Therein, the purity of the graphene layer, as well as the shape, strongly influenced the ability of the graphene sheet to scroll. Plus, incomplete scrolling was observed either due to the difference in solvent evaporation rate against the scrolling rate or the system requiring further solvent application and evaporation steps in order to overcome the initial energy barrier associated with the first stage of scrolling. The scrolling event can be stabilized by the $\pi-\pi$ interaction of the overlapped regions of the graphene layer.[89] The use of surfactants with pure graphenes has limited impact on the nano- to microscale architecture through direct influence. However, the use of surfactants may be warranted where the architecture of individual pristine (hydrophobic) graphene sheets has already been changed and rapid or facile assembly of a micro to macro-level device is

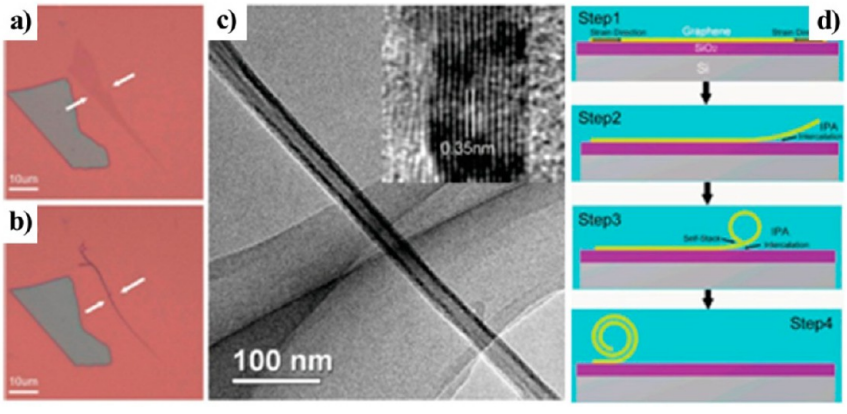

Figure 6. Surface tension-induced scrolling of graphene layers through evaporation of solvents from the graphene surface, where (a) the graphene sheet is initially in the planar state, but (b) on solvent evaporation, the same graphene sheet is observed to have reduced in apparent surface area. (c) Under transmission electron microscopy, the scrolled nature of the graphene sheet is evident, with basal plane separation of around 0.35 nm similar to that of graphite stacking and multiwalled carbon nanotubes (inset). (d) Schematic representation of the scrolling mechanism of graphene layers drying from isopropyl alcohol solution. Reprinted from ref 89. Copyright 2009 American Chemical Society.

warranted. Therein, the minimal effect of surfactants on graphene architecture ensures preservation of the initial structure in the final stage.[94] While this may be acceptable for certain application purposes, residual surfactants are not easily removed from carbon nanomaterials,[95] and may lead to a decrease in electrical performance depending on the type of surfactant used.[96]

Rolling of pure graphene layers can also be achieved by the exertion of an electrostatic field during the exfoliation and deposition of graphenes in the presence of appropriate atomic species. Akin to the mechanism for edge stress induced conformational changes of graphene, electric fields lift graphene sheets from the substrate surface and, given the correct atmosphere, also introduce adatoms to the graphene sheet. The combination of these two factors is sufficient to cause scrolling, where the adsorption of species, such as hydrogen atoms, induces stress on the graphene lattice.[91]

The presence of oxygen groups on the graphene surface introduces additional effects when considering forces directly enacting on SLGO. SLGO can be stably suspended in a variety of solvents, which is not reflected in the pure graphene system, making SLGO more attractive in terms of processability.[72] The colloidal stability of SLGO is directly inferred from functionalized regions that render areas wettable and proffers intersheet repulsion.[56] The surface charges can be overcome by adjusting the pH of solution or increasing the concentration of salt, where destabilization of the surface charges in this manner results in precipitation of SLGO from solution, which has been useful when applied toward size separation of graphenes.[97] The effect of pH on SLGO stability is more dramatic when considering the change in architecture.

The total number of oxygen-containing functional groups (including carboxylic, lactone and phenolic environments on the carbon surface that are capable of titrating)[98] varies according to the study and technique used. For example, for one type of SLGO, the total number of oxygen-containing groups was found through acid−base titration analysis to be *ca.* 7.5 mmol g^{-1}.[61] Additional oxygen-containing functional groups are identified through XPS[99] or solid-state NMR,[56] which include tertiary hydroxyl groups and are considered the dominant type of groups on SLGO. However, these groups are not readily identified by titrations, although it is possible to titrate tertiary hydroxyl groups using acetic anhydride/pyridine reagent and titrate with methanolic potassium hydroxide for secondary and tertiary hydroxyls groups (and using *p*-toluenesulfonic acid instead of pyridine if the hydroxyl groups are hindered). Direct comparisons between XPS studies and titration analysis of the carbon−oxygen environment is difficult.[100] The distribution of oxygen-containing groups on SLGO is random, due to the indiscriminate positioning of lattice defects in the carbon lattice and regions where acid oxidation occurs, though carboxylic and tertiary hydroxyl groups can only be sited at the periphery or at the edge of in-sheet holes (Figure 7).

The increase in pH of the chemical environment causes deprotonation of the oxygen-containing acidic groups in the SLGO, which establishes a negative surface charge density and renders the groups more hydrophilic. The zeta potential of SLGO sheets is below −30 mV when the pH is less than 3 and can reach −45 mV when the pH approaches 10.[56,102] When the zeta potential is more negative than −30 mV, the graphene has sufficient charge to repulse neighboring graphene sheets and maintains a stable dispersion. Thus, SLGO has increasing stability of suspension as the pH is increased from 3 to 14. When SLGO is placed in an acidic environment, the oxygen-containing groups are fully protonated, and therefore, intersheet repulsion decreases, causing precipitation of SLGO from solution. The pH-dependent colloidal behavior and structure of SLGO mimics that of a humic acid, where the material is stably suspended at high pH, but precipitates from solution at low pH. Graphene oxide can therefore be considered as the largest known humic acid structures.

In low pH solution, SLGO is observed, using TEM, to appear stacked and many cases folded, though the overall architecture is flat (Figure 8a). Therein, SLGO behaves in a similar fashion to fulvic acids, which become stably immobilized on graphitic surfaces at low pH. It is possible to conceive that regions of functionalized graphene can interact with other areas of the same graphene sheet, as well as different graphene sheets, at low pH environments, thus causing folding events. The hydrophobic areas of SLGO are minimized to the surrounding solution. As the pH is increased above neutral, negative charges on the oxygen groups will cause repulsion between closely neighboring oxygen containing groups, causing the sheet to morph from a planar arrangement (Figure 8b) to a curved state (Figure 8c). With the high number of oxygen groups present on SLGO, there are many focal points for radial curvature; therefore, folding does not operate along a single axial plane across the length of the sheet. TEM images of SLGO dried from a high pH environment reveal the graphene sheets to have crumpled or collapsed through multiple bends and folds, often into star-like formations, in complete contrast to SLGO in low pH or neutral pH solution. Therein, these collapsed structures reduce the interface between unfunctionalized regions of SLGO.[102,103] It is worth noting that surface tension forces act on SLGO as it dries from the surrounding environment during TEM preparation and therefore experiences a degree of additional change in its architecture; however, this has only been observed to exacerbate changes that have already occurred as a result of pH given that the crumpled or star-like nature of SLGO has only been observed when SLGO is subjected to high pH environments. The collapse

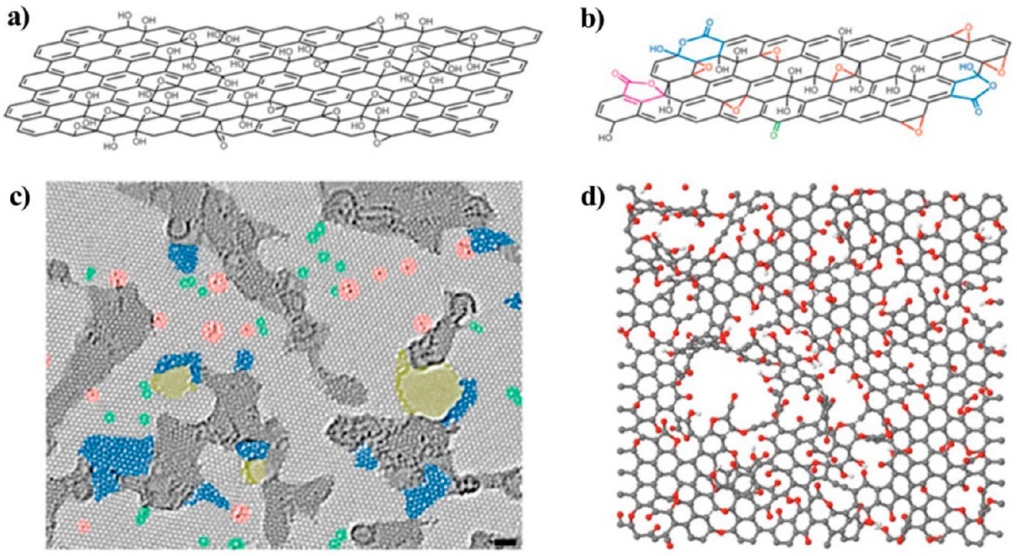

Figure 7. Models of oxygen-containing groups distribution on the surface of single layer carbon. (a) The model assembled from the Lerf-Klinowski and He studies on graphite oxide. (b) An updated model for graphite oxide. (c) False color rendered atomic resolution, aberration-corrected high-resolution transmission electron image of a single-layer reduced graphene oxide membrane, where dark gray regions indicate contaminated graphene, blue regions highlight lattice defects or disordered graphene, red regions reveal single atom substitutions and yellow regions show in sheet holes (scale bar 1 nm). (d) A model of SLGO combining recent studies to include defects, holes and oxygen groups distributed throughout the graphene layer. Reprinted with permission from refs 70, 71, and101. Copyright 1998 Elsevier, 1998 American Chemical Society Publications, and 2010 Nature Publishing Group.

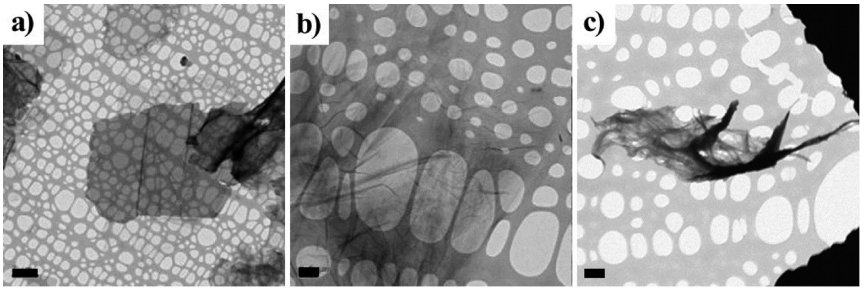

Figure 8. TEM images of SLGO dried from buffered solutions with pH of (a) 2, (b) neutral, and (c) 12. Scale bar = 2.0, 0.5, and 0.5 μm, respectively. Reprinted with permission from ref 102. Copyright 2011 Royal Society of Chemistry.

of SLGO at high pH has been demonstrated to trap silver nanoparticles (Figure 9). The mechanism of SLGO collapse at high pH was also determined to be reversible by switching the solution from a high to a low pH. Scanning electron microscopy images of SLGO, immobilized on carbon nanotube buckypaper, showed SLGO in "open" and "closed" states depending on the final pH from which the system is dried.[102]

Graphene Architecture through Template Interaction. Numerous methods exist in the synthesis of graphene-based three-dimensional macrostructures, including template,[104] cross-linking through polymer support,[105] and direct chemical vapor deposition.[106] The use of other nanomaterials has also facilitated the change in architecture of graphenes, which are capable of conforming their structure over a three-dimensional template to induce architectural changes and whereby the nanomaterials also prevents complete collapse of the graphene sheets.[107] The drying of the system at elevated temperatures can lead to partial reduction of graphene oxide through removal of the oxygen groups, although it is possible to retain the full SLGO state and its chemistry through the application of inert gas. In the layering of the graphene sheets around a template, the sheets can be induced into overlap of the $\pi-\pi$ bond network and interaction of attractive van der Waals forces, which stabilizes the macroscale architecture similar to the stacking arrangement in graphite and multilayer graphene.[105,108,109] Therein, the chemical environment can be exploited to overlap graphene sheets and further manipulated to extend the size of the graphene system, where control may be maintained over the graphene sheet architecture and the overall system.

Graphene-based systems, often with hierarchical ordering, have been assembled using nano- or microscale templates, such as polymers,[111−114] emulsions,[115] gold,[116] magnetite,[117] silica,[118,119] titania,[120,121] calcite,[122]

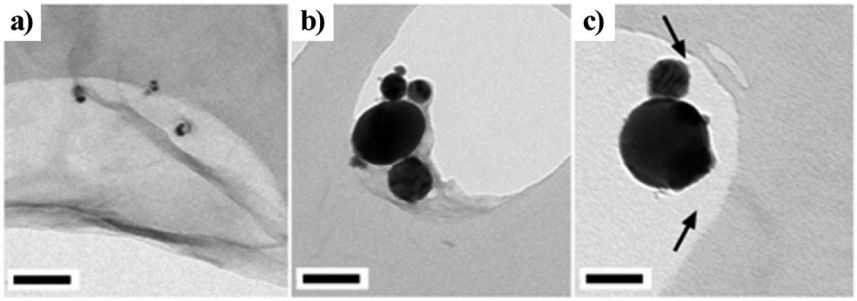

Figure 9. Changes in the chemical environment of graphene oxide lead to structure changes. (a) Graphene oxide in a low pH solution maintains the graphene oxide sheets in a planar arrangement where silver nanoparticles (AgNPs) can rest on the surface. (b) In high pH solution, graphene oxide sheets collapse, which leads to envelopment of AgNPs, which are (c) sometimes observed to be fully suspended over the holes in the TEM grid supported by the graphene sheet interaction with the TEM grid support film. Scale bars = 100 nm. Reprinted with permission from ref 102. Copyright 2011 Royal Society of Chemistry.

tin,[123] tin oxide,[124] zinc oxide,[125] lithium vanadate,[126] and ice.[26,104] Graphene platelet precursors have been mixed with latex nanospheres and surrounded by a latex host to form three-dimensional structures.[110] The system relies on graphene adhesion to latex nanoparticles and significant overlap of neighboring graphene sheets to form a conductive network, which are dried in place leading to the (near) hexagonal framework of graphenes distributed in the latex host (Figure 10). This generated a system with a low percolation threshold (0.1 vol %) and an electrical conductivity of 217 S m^{-1} when a 6 vol % loading was used (though this system was built from multilayer graphene, which may indicate a higher electrical conductivity than monolayer graphene). Therein, the intrinsic architecture of graphene does not change substantially, but the approach demonstrates the feasibility of creating three-dimensional networks through partial overlap of graphene sheets. Use of the "breath figure" method has also lead to formation of interconnecting graphene networks, where polymer grafted graphene oxide sheets were dispersed into an organic solvent and then evaporated under a stream of humid air, allowing condensation and close packing of the graphene layers. The resulting flexible film is porous, with the pore dimensions controlled by the graphene oxide concentration and the polymer chain length. The inclusion of nitrogen-doped graphene results in films with a conductivity of 649 S·cm^{-1}.[127]

The use of graphenes has also been applied to preformed three-dimensional templates.[128,129] These have also been used to support the growth of graphene (for example, see ref 130); however, this paper is only considering the flexibility of already formed graphene adapting its architecture to templates. Reduced graphene oxide was added to a polyurethane foam by a vacuum degassing method and then heat treated in a closed vessel. On drying, the "polymer-based graphene foam" exhibited excellent compressibility (up to 90% with full recovery of shape) and without delamination of the polymer backbone.[129] Herein, graphene sheets are observed to follow the contours of the polymer

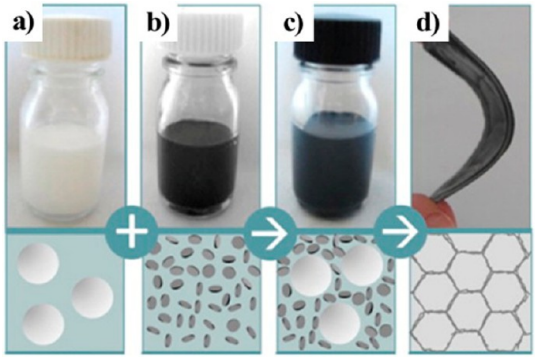

Figure 10. Processing steps of the nanocomposite materials involved (a) blank latex and (b) nanosized multilayered graphene (NMG) suspension, (c) where the NMG is introduced dropwise to the latex suspension to promote greater adhesion between the graphene and latex particles. (d) A flexible and conductive material obtained after water evaporation and film formation. Reprinted with permission from ref 110. Copyright 2014 Elsevier.

matrix. Sacrificial templates have also been used to synthesize three-dimensional graphene architecture.[131,132] In one embodiment, calcium chloride powder is first dissolved and mixed with a dispersion of graphene oxide. The mixture is then dried, giving graphene a physical template of calcium chloride and also allowing overlapping graphene to partially stack, promoted by surface tension forces acting on the graphene sheets under evaporation of the solvent. The graphene was reduced in hydrazine vapor and the calcium chloride was finally removed to give an open three-dimensional array (Figure 11).[132]

Three-Dimensional Interconnectivity of Graphenes through Hydrothermal Treatment and Coagulation. Three-dimensional arrays of graphene have also been successfully produced in the absence of a nanomaterial template for hydrogels,[105,133−137] hydrothermal treatment (often incorporating a chemical reduction of graphene oxide to graphene),[138−141] and electrochemical reduction.[142] These systems predominantly involve self-assembly processes, yielding structures with high compressibility and the latter two techniques leading to electrically

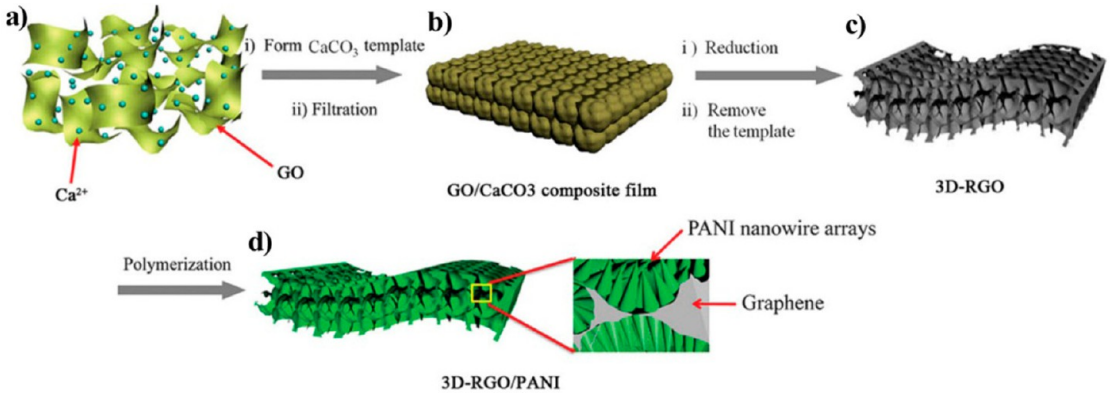

Figure 11. Chemical synthesis mechanism of three-dimensional graphene oxide networks extended into hierarchical ordered arrays with polyaniline. Reprinted with permission from ref 132. Copyright 2013 Wiley-VCH Verlag GmbH.

conductive systems and higher mechanical stability. Hydrothermal treatment reduces the oxygen environment of graphene oxide leading to hydrophobic domains, which are combined with $\pi-\pi$ interactions leading to a random stacking of graphenes in 3 dimensions. The final system contains submicrometer to several micrometer sized pores, where the graphene sheets have contorted their structure to provide a robust interconnected network.[138] It was also demonstrated that once the three-dimensional graphene array was formed, it was possible to use the structure as a template to generate graphene composite structures. The system featured superelastic, conductive and stimuli-responsive properties.[24]

Graphene architecture can be forced to change through external stimuli. Aqueous dispersions of large graphene oxide sheets were injected into spinning coagulation baths to form fibers. Within the fibers, the graphene sheets are aligned with the flow direction, but locally aligned graphene regions reside at different orientations to neighboring systems, often where graphene sheets are observed with "dentate" bends formed during the dehydration of the gel fibers. While these fibers are tightly packed systems using calcium chloride (5 wt % $CaCl_2$ in ethanol/water) or sodium hydroxide (5 wt % NaOH in ethanol/water) as the coagulant, it is possible to generate porous fibers when using potassium hydroxide (5 wt % KOH in ethanol/water) or low concentrations of calcium hydroxide (1 wt % $CaCl_2$ in ethanol/water).[143] When injecting graphene oxide gel (by centrifuging a graphene oxide dispersion) into liquid nitrogen, the frozen fibers were freeze-dried then vacuum-dried to produce electrically conductive aerogel fibers with aligned pores.[144] The graphene sheets overlap and have undergone significant bending within the fiber to maintain a porous architecture.

A hydrothermal treatment (180 °C) of graphene oxide and a biomass or a polymer followed by potassium hydroxide activation[145,146] (at 800 °C) resulted in a porous, three-dimensional graphene material exhibiting a specific surface area of 3523 $m^2 \cdot g^{-1}$ (Figure 12a),[147] which is slightly higher than activated carbon aerogels *ca.* 3431 $m^2 \cdot g^{-1}$,[148] albeit less than a zinc-mediated coordination copolymerization of a dicarboxylic and tricarboxylic acid with a specific surface area of 5200 $m^2 \cdot g^{-1}$.[149] Electron microscopy reveals that the graphene architecture is highly contorted, where the carbonized biomass or polymer provides a physical support in the separation of individual graphene layers (Figure 12b–e). The sample also has a conductivity up to 303 $S \cdot m^{-1}$.

Oxygen Group Reactions on Graphene. There are a growing number of articles highlighting key research on sheet chemistry of single-layer graphene and graphene oxide, which are captured in existing reviews.[14,33,150–152] It serves to indicate such reviews and highlight key developments pertaining to conformational changes of SLG and SLGO and elucidate possible driving mechanisms.

Covalent bonding of atoms to the basal plane of graphene introduces lattice strain, given the change in hybridization of carbon bonds from sp^2 to sp^3, which can be minimized by conformational changes known as "geometric relief".[153] The creation of an unpaired electron at the site adjacent to the covalently attached atom is combined with a change in the surrounding electron density due to the structural deformation, leading to enhanced chemical reactivity. It is possible that the lattice strain is propagated through the graphene structure, using a similar mechanism to that of edge strains, which will lead to changes in graphene structure over a larger region. Moreover, the introduction of dislocation densities can affect the mechanical performance of graphene, where the type, distribution and density can alter the fracture strength of the sheet.[154]

The structure of SLGO, as described above, possesses numerous oxide groups around the periphery and across the surfaces of graphene. These represent key groups potentially capable of chemically reacting. However, the initial focus of chemistry as applied to SLGO appears predominantly to be to drive graphene

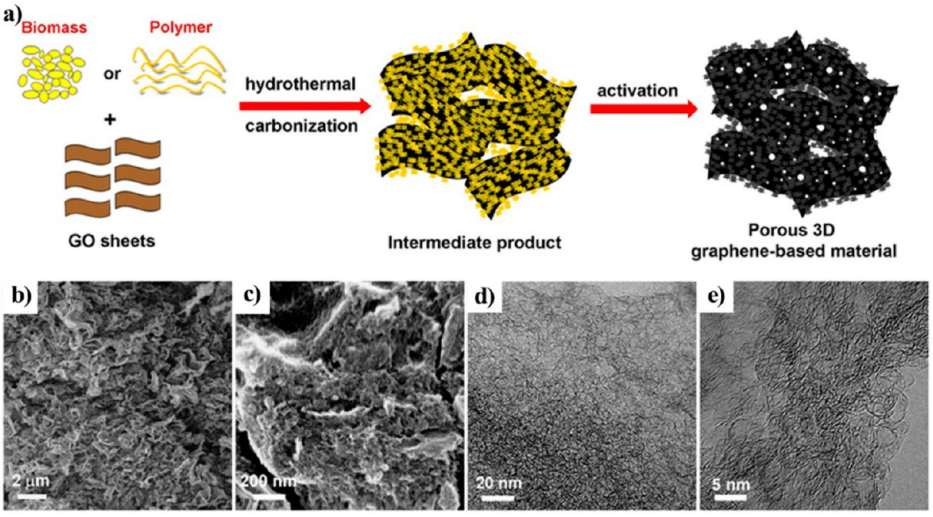

Figure 12. (a) Assembly mechanism and (b–e) scanning electron microscope images of a porous 3-dimensional graphene material exhibiting high specific surface areas. Reprinted with permission from ref 147. Copyright 2013 Nature Publishing Group.

oxide through reduction processes in order to remove oxygen-containing groups and obtain SLG or SLGR with properties of pure graphene. Hydrazine reduction has been used extensively toward this goal,[57] though many other reductant chemicals are also possible depending on the synthesis conditions and final state of the graphene required.[155] SLGO, which is initially beige and stably suspends in aqueous solution, turns black and hydrophobic on reduction. The carbon to oxygen ratio increases from 2.7:1 to 10.3:1, implying a removal of oxygen-containing groups and XPS analysis confirms a significant drop in the intensity of carbonyl, epoxy and carboxylic type groups after reduction. The proposed mechanism is an epoxide reduction where double bonds of the graphene layer are restored. When compared with Boehm titration analysis of hydrazine-reduced SLGO (SLGR), under the same conditions, the starting amount of carboxylic groups, for example, drops by only 20%, which is sufficient to increase the hydrophobicity of the graphene sheet and it was not possible to suspend the sample in water. This raises questions as to whether other studies used SLGO without the removal of fulvic acids, which are easier to chemically reduce and may give higher apparent loss of oxygen groups. The remaining carboxylic groups can undergo further chemical modification, but it has been that the chemical reduction treatment weakens the graphene lattice. Acylation of hydrazine-derived SLGR in thionyl chloride causes a further loss of the number of carboxylic groups, after reduction, by *ca.* 60%.[61]

SEM images reveal that the structure of hydrazine-reduced SLGR is often dissimilar to that of the original starting material where the graphene sheets are reduced in size due to erosion of the lattice, stacked and folded (Figure 13). Therein, incomplete reduction may leave covalently bound atoms on the surface of the SLGR, which assist the folding process in order to

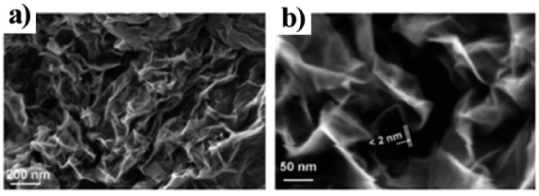

Figure 13. SLGO reduced by hydrazine to SLGR leaving the graphene structure to have (a) crumpled and (b) fold dimensions of around 2 nm. Reprinted with permission from ref 57. Copyright 2007 Elsevier.

relieve lattice strain. It is also possible that the reduction process partially etches the graphene sheet leading to a weakened structure, which could be used as a site for folding and SLGR appears to be as flexible as SLGO.[156] Nonetheless, the conductivity of hydrazine-reduced graphene oxide is 2400 $S \cdot m^{-1}$, compared with SLGO of 0.021 $S \cdot m^{-1}$,[57] where there is restoration of the graphene structure.[157]

When SLGO is immersed in solutions containing divalent metal ions, wrinkling or folding and stacking occurs, depending on the concentration of both species. A divalent metal ion, such as copper(II), can interact electrostatically and coordinate with carboxylic groups on SLGO with the possibility of linking two different sites on the graphene sheet to the same locale. When the carboxylic groups are saturated, the electrostatic repulsion between other carboxylic groups are reduced, leaving the system to interact through the $\pi-\pi$ bond network and stacking ensues.[158]

Stacked and folded graphene structures were also observed when reacting SLGO directly with thionyl chloride and subsequent treatment with an aliphatic or aromatic amine. The initial acylation conditions of the carboxylic groups occur under reflux at *ca.* 90 °C, which is sufficient to render the SLGO black and precipitate from suspension. It is possible that erosion

of the graphene oxide lattice occurs under these harsh conditions; however, assessment of the number of carboxylic groups before and after the amidation reaction revealed SLGO-acyl chloride reactivity was 83% and 67% toward aliphatic and aromatic amines, respectively. Steric hindrance from the aromatic amine was indicated as a likely limitation, but electrostatic bonding and folding of the graphene sheet may also be possible factors.[61]

An alternative approach to achieve amidation of SLGO is the use of carbodiimide reactions.[159−161] Carboxylic groups on SLGO can be modified with a carbodiimide, such as 1-ethyl-3-(-3-(dimethylamino)-propyl) carbodiimide (EDAC), to form an *O*-acylisourea intermediate. This can be further modified with *N*-hydroxysuccinimide (NHS) to yield an NHS ester, which can then react with amine groups to form amide coupling without experiencing unwanted side reactions. When reacting EDAC with a stable suspension of SLGO, the concentration of EDAC can cause SLGO to precipitate from solution. However, the event is not strictly limited to only salting out of the graphene layers. TEM images of EDAC-reacted graphene show that the graphene layers have crumpled into star-like formations, which explained the low reactivity from the intermediate to the final amide when using glutamic acid.[61] Therein, salting out of graphene layers from solution would not directly lead to alteration of the graphene architecture;[61] therefore, the reaction with EDAC, prior to addition of NHS, to form the *O*-acylisourea intermediate may further react with vacant carboxylic groups on other regions of the SLGO sheet leading to intrasheet bridging, resulting in sheet collapse, evident from TEM images. It was possible to reduce the concentration of EDAC (and NHS) in a solution of SLGO such that salting out does not occur and SLGO remains suspended. Therein, the SLGO−NHS intermediate was reacted with ferritin, which was confirmed using TEM, which revealed that ferritin was added across the surface and along the periphery of the graphene sheets. Moreover, even with a reduced concentration of EDAC and NHS, the edges of SLGO were curled, suggesting intrasheet bridging was still occurring, but to a much lesser extent.[162]

Intra- and Inter-Sheet Bridging Chemical Reactions of Graphene. Structural changes of graphene sheets, in particular SLGO, have been reported to be affected by chemical reactions. Therein, the extent of architectural change depends not only on the bond formed between the reacting chemical and surface groups on graphene, but also on the type of interaction between the graphene sheet and the remaining structure of the reacting species. Isocyanate reactions with graphene oxide systems have been published, where carboxylic and hydroxyl groups provide suitable covalent bonding sites to the isocyanate molecule.[163−166] Diisocyanates, however, provide two (generally speaking) chemically equivalent sites capable of bonding to certain oxygen groups on SLGO. When using aromatic diisocyanates, typically 2,4-diisocyanato-1-methylbenzene, the resulting graphene sheets appear planar and stacked. However, when using linear aliphatic diisocyanates, such as 1,6-diisocyanatohexane, then the graphene layers are contorted into star-like formations.[156] It was deemed that the aromatic diisocyanate molecules could adsorb to the surface of SLGO combined with potential steric hindrance of the isocyanate groups preventing both groups reacting with graphene, leading to retention of the planar structure of graphene and stacking through van der Waals and $\pi-\pi$ bond interactions between adjacent sheets. However aliphatic diisocyanate molecules would be unrestricted in reaction at either termini with different sites of the graphene sheet, potentially leading to intrasheet bonding, induced curvature and folding.

With either molecule, not every isocyanate termini will be fully reacted, assuming no termination species is added to the reaction, which leaves potential sites to conduct further chemistry. The attachment of a pyrrole unit to SLGO-diisocyanate was effected, allowing the polymerization of pyrrole to extend away from the SLGO sheets.[156] When using an insoluble polypyrrole polymerization route, particles of polypyrrole were found to decorate both aliphatic and aromatic diisocyanate modified SLGO. The underlying architecture of the graphene sheets remained in the configuration as generated by their reaction with the diisocyanate molecules. Herein, the change in architecture was solely due to the diisocyanate reaction and appeared unaffected by subsequent polymerization of pyrrole. To confirm that covalent attachment had taken place between polypyrrole and SLGO, a soluble polypyrrole polymerization route was used, allowing free polypyrrole to be washed away from the system, which revealed that polypyrrole particles remained adhered to the surface of graphene.

To elucidate the impact of graphene architecture in composite systems, polypyrrole attached SLGO, resulting from either aliphatic or aromatic diisocyanate, was compressed into a pellet, and its electrical property was investigated. When all other parameters were kept the same (*i.e.*, mass of SLGO, molar ratios of reactants, reaction conditions, *etc.*), it was found that when SLGO was in a tightly contorted (aliphatic diisocyanate) formation, the composite had a lower resistivity than when SLGO was in a planar state (aromatic diisocyanate), albeit both systems had higher resistivities than pure polypyrrole. SLGO acts an electrical insulator,[167] and therefore, the extent of its deformation from a planar state can lower its apparent surface area, and thus limit the number of interruptions along the path length.[156]

Graphene architecture, once transformed through an initial chemical reaction with, for example, diisocyanate,

molecules can be further manipulated through additional chemical reactions. Graphene (as SLGO) when reacted with diisocyanates form different architecture depending on the linker chemical between isocyanate groups.[156] The addition of a diamine to the graphene–diisocyanate mixture forms polyurea and in the case of an aliphatic diisocyanate and diamine reaction on graphene transforms the crumpled architecture into a highly interconnecting web-like system (Figure 14a), which can be further functionalized through the chemical attachment of biomolecules, such as ferritin (Figure 14b).[162] These architectural changes take place in solution and are maintained during drying to their final form, which was confirmed by critical point drying (Figure 14c) to avoid additional structural changes brought about by surface tension forces acting on the graphene structure through drying.[168] This leads to an ability to manipulate and preserve the graphene architecture during various stages of wet chemistry and its potential inclusion into host systems. Plus, chemical functionalization with biological molecules extends the usefulness of graphene toward biological and biomedical applications.[169]

To achieve greater control over graphene-based porous architecture, it was found that use of metal salts (Au, Ag, Pd, Ir, Rh, or Pt chlorides) would interconnect anionic groups, leading to intrasheet or intersheet bridging of graphene during hydrothermal treatment (Figure 15a). The pores ranged in size but could reach up to 10 μm (Figure 15b).The presence of metals on graphene was important in the formation and physical retention of the three-dimensional architecture and, when removed, led to near full collapse. The added advantage of this approach is the retention of metal nanoparticles within the graphene system, which exhibited high catalytic activity in the Heck reaction.[170] Graphene hydrogels yield a similar open pore architecture, where the graphene sheets are first functionalized with polymer chains and then cross-linked (Figure 15c). Therein, changes in graphene architecture are less pronounced than the hydrothermal treatment systems and the polymer interconnections reduce the thermal stability of the system.[105,133] Moreover, the internal porous arrangement (Figure 15d), while still open, is often smaller than its hydrothermally treated counterparts.

Graphene and graphene oxide have been used to support the presence of nanoparticles for a variety of applications and in many cases exhibit a synergistic relationship yielding superior (and tunable) chemical properties than either component separately. This has been important for battery,[171] photocatalysis,[172] fuel cell,[173] oxygen reduction or evolution catalysis,[174] biosensor,[175] optoelectronic,[176] drug delivery, imaging and diagnostic[177] applications. Often this requires the graphene–nanoparticle composites to be held in a three-dimensional matrix, thus keeping access to the

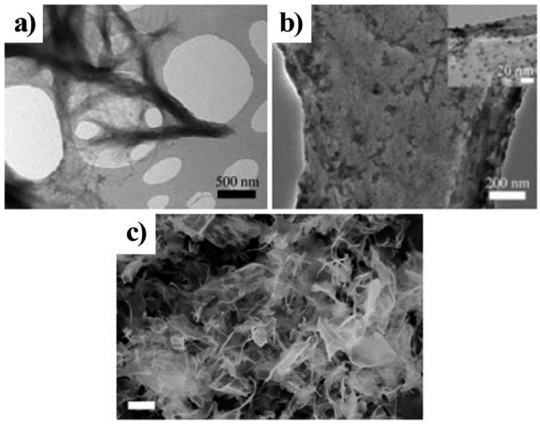

Figure 14. SLGO–polyurea composite from aliphatic diisocyanate and diamine reaction leading to (a) web-like interconnected architecture in TEM, which can be (b) further functionalized through the attachment of ferritin molecules to residual oxygen-containing groups on the three-dimensional graphene structure. Ferritin molecules are observed decorating the surface and scroll edges (inset). (c) Scanning electron microscopy images reveal that the three-dimensional structure is preserved under critical point drying, and therefore, the graphene architecture is formed and can be preserved in solution (scale bar = 10 μm). Reprinted from ref 162. Copyright 2013 American Chemical Society.

reactive sites open. Graphene has a theoretical specific surface area (SSA) of *ca.* 2630 $m^2 \cdot g^{-1}$,[14] though in preparation for analysis graphene and in particular graphene oxide collapses into a stacked structure with an SSA of *ca.* 50 $m^2 \cdot g^{-1}$,[103,166] which is in the range for exfoliated graphite.[178] Obtaining the high surface area would be useful for sorption or mass transfer processes, as long as the intervening architecture between the sorption site and the main stream is readily accessible.

Reduction chemistry has also been employed in the formation of three-dimensional macrostructures of graphene, where graphene oxide was simultaneously reduced by use of oxalic acid and sodium iodide.[179] The removal of oxygen-containing groups from SLGO produces increasingly hydrophobic graphene sheets, which tend to agglomerate.[180,181] This brings graphene sheets into closer proximity, where hydrophobic and $\pi-\pi$ bonds interactions can stabilize the macrostructure, but also enable cross-linking between different neighboring graphene sheets. The resulting architecture is a porous network, a graphene aerogel (Figure 16a), which has high electrical conductivity, low density and good mechanical strength (Figure 16b). While this may not be the least dense graphene material,[182] this elegantly demonstrates how chemistry may be used to directly manipulate and control the three-dimensional architecture of graphene. Nonplanar graphene-based composites, derived from chemical modification, have been found useful for oil and organic solvent adsorption,[183] batteries,[184] supercapacitors,[185] solar cells,[186] sensors,[187] and chemical oxidation.[188]

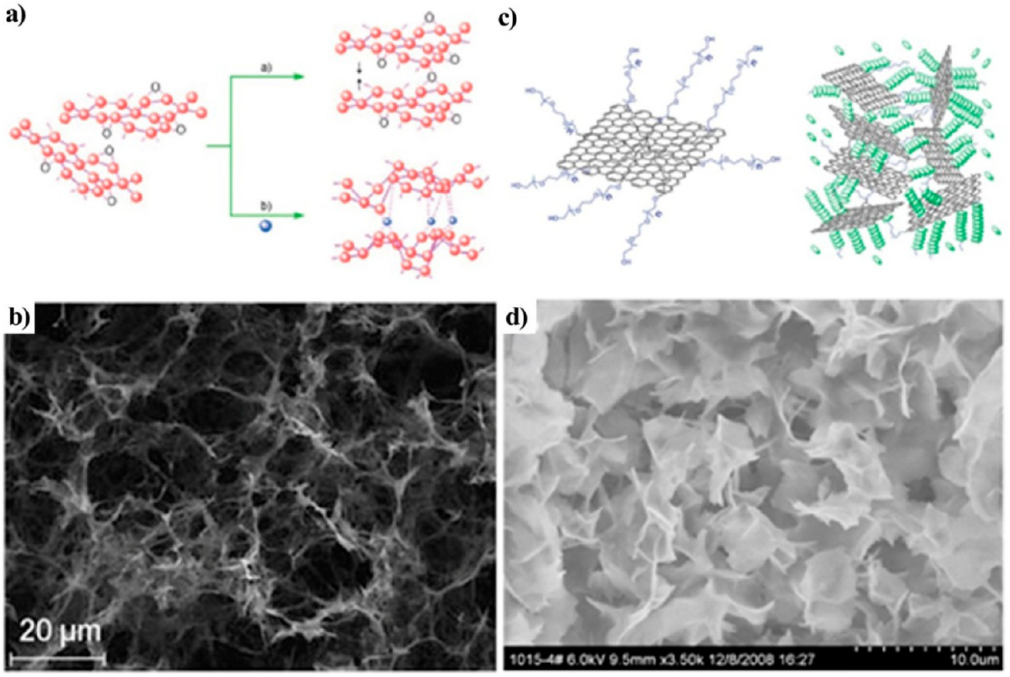

Figure 15. (a) Metal ion promoted bridging of graphene sheets influences (b) the porous architecture of graphene arrays produced by hydrothermal treatment, leading to large diameter pores. (c) The functionalization of graphene with polymers can then be cross-linked into (d) an open porous graphene–polymer composite. Reprinted with permission from refs 105 and170. Copyright 2009 American Chemical Society and 2010 Wiley-VCH Verlag GmbH.

Graphene Architecture Affecting Properties. Regardless of the methodology used, the use of chemistry can effect changes to the architecture of preformed graphene, which can be carried through to graphene-based composites. The degree to which its properties can be altered depends principally on the final structure of the graphene and/or the graphene-composite and is therefore linked to the chemistry utilized (Table 1).

Chemical moieties can effectively separate graphene layers to form porous frameworks, based on metal oxide frameworks, which can yield a surface area up to 933 $m^2 \cdot g^{-1}$.[10] Nanomaterial templates have generated three-dimensional structures with surface areas up to 1159 $m^2 \cdot g^{-1}$.[118] However, the highest surface area of a graphene-based material comes from the chemical activation of graphene using potassium hydroxide followed by hydrothermal treatment with biomass or polymer spacers, yielding a surface area of 3523 $m^2 \cdot g^{-1}$.[147] The latter also possesses a specific capacitance of 231 $F \cdot g^{-1}$ at 1 $A \cdot g^{-1}$. It has been recorded that nanomaterial templates followed by hydrothermal treatment to stabilize the macro-structure lead to a higher specific capacitance of 362 $F \cdot g^{-1}$ at 1 $A \cdot g^{-1}$.[132] The highest specific capacitance was tested at 2815 $F \cdot g^{-1}$ at 1 $A \cdot g^{-1}$, where graphene oxide sheets were layered around sacrificial silica templates, thermally reduced and then loaded with nickel hydroxide nanoparticles.[118] Therein, graphene sheets form the porous three-dimensional framework that facilitates electron transport and electrolyte ion movement. Control over the three-dimensional architecture is vitally important in battery applications, where graphene can provide a framework for active sites for charging and discharging events. A graphene-based lithium–air electrode was recorded with a high discharge capacity of 15 000 $mAh \cdot g^{-1}$ and a specific capacity of 5000–15 000 $mAh \cdot g^{-1}$ at a current density of 0.1 $mA \cdot cm^{-2}$.[184] Therein, the hierarchical porous structure was developed through the interlinking of functionalized graphene sheets and a PTFE binder, but yielded a surface area of 186 $m^2 \cdot g^{-1}$, far below the theoretical level for graphene. This approach to three-dimensional graphene structures did exhibit a conductivity of 20 000 $S \cdot m^{-1}$. A highly contorted array of graphenes in a fiber was cast in a coagulation bath and then chemically reduced in hydrazine vapor after drying. The tensile strength and Young's moduli of the fibers derived by use of different coagulation baths was measured at 501.5 and 11 200 MPa, respectively.

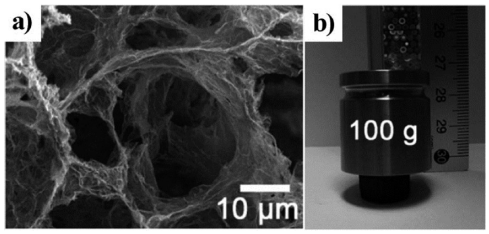

Figure 16. A graphene aerogel from oxalic acid and sodium iodide reduction and cross-linking reaction, (a) capable of freely supporting a mass and (b) SEM image revealing the open porous network of graphene. Reprinted with permission from ref 179. Copyright 2012 Royal Society of Chemistry.

TABLE 1. Comparison of Properties from Chemically Controlled Graphene Architecture

	surface area (m^2/g)	specific capacitance at 1 A/g (F/g)	reversible capacity (mA h/g)	conductivity (S/m)	tensile strength (MPa)	Young's modulus (MPa)	ref
Porous graphene oxide - boronic acid frameworks	470						Srinivas *et al.*[8]
Graphene - benzene-1,4-diboronic acid MOF	470						Burress *et al.*[9]
Graphene-Porphyrin MOF	933						Jahan *et al.*[10]
Rippled reduced graphene oxide paper				8100			Dikin *et al.*[20]
Co-continuous graphene networks in poly(propylene carbonate)					33 @ 20 °C	5500 @ 20 °C	Gao *et al.*[29]
Co-continuous graphene networks in poly(propylene carbonate)					5 @ 75 °C	500 @ 75 °C	Gao *et al.*[29]
2-dimensional graphene paper				16000			Park *et al.*[72]
Crumpled graphene balls	567	105					Luo *et al.*[94]
Hierarchical graphene in latex				217			Noel *et al.*[110]
3-D graphene from polystyrene sacrificial template	194.2	389					Choi *et al.*[111]
3-D graphene from polystyrene sacrificial template	339	58.4					Wang *et al.*[113]
3-D graphene from polyoxometalate nanoparticle template	680			536			Zhou *et al.*[114]
Graphene-encapsulated hollow Fe_3O_4 nanoparticles	132		900 @ 100 mA·g				Chen *et al.*[117]
Nickel hydroxide-coated 3D porous graphene hollow sphere framework	1159	2815					Zhang *et al.*[118]
Porous graphene film from silica sacrificial template	231.4	322.3					Kim *et al.*[119]
3-D structured titania template	180.8						Yan *et al.*[121]
Hierarchical porous reduced graphene oxide from $CaCO_3$ sphere template	540	201 @ 0.1 A/g					Gu *et al.*[122]
Interconnected 3-D graphene networks using tin templates	365		865 @ 0.5 C				Qin *et al.*[123]
Porous graphene networks from tin oxide template (SnO-graphene)	354.6		337.5 @ 200 mA·g				Zhou *et al.*[124]
Porous graphene networks from tin oxide template (SnO-carbon-graphene)			843.3 @ 210 mA·g				Zhou *et al.*[124]
Hollow structured Li_3VO_4 wrapped with graphene nanosheets			223 @ 20 mA·g				Shi *et al.*[126]
N-doped graphene hierarchical structures from breath-figure method		103.2		64900			Lee *et al.*[127]
Graphene network from preformed 3-D silica template	347						Niu *et al.*[128]
Graphene network from preformed 3-D polymer template				0.22			Wu *et al.*[129]
Porous reduced graphene oxide film from $CaCO_3$ template	116.2	362					Meng *et al.*[132]
Porous 3-D graphene hydrogel	220						Compton *et al.*[135]
CO_2-activated, hierarchical trimodal porous graphene frameworks	829	157.7					Yun *et al.*[136]
Self-assembled graphene hydrogel with hydrothermal treatment		160		0.5			Xu *et al.*[138]
Free standing paper like graphene foam		110			3.2	7—40	Niu *et al.*[139]
3-D reduced graphene oxide hydrogel with TiO_2 template	155		197 @ 0.5 C				Yu *et al.*[141]
Reduced giant graphene (RGGF-Ca^{2+}) 3-D fibers				41200	501.5	11200	Xu *et al.*[143]
Porous graphene fibers	884			4900		350	Xu *et al.*[144]
Porous microwave exfoliated graphene oxide	3100	200 @ 0.7 A/g		500			Zhu *et al.*[145]
Free standing porous graphene films	2400			5800			Zhang *et al.*[146]
Porous 3-D graphene material	3523	231		303			Zhang *et al.*[147]
3-D delaminated graphene nanosheets and SnO_2			810 @ 50 mA·g				Paek *et al.*[171]
3-D graphene assemblies by chemical reduction	151			24.8			Zhang *et al.*[179]
Hierarchically porous graphene	186		5000 @ 0.1 mA·cm^2	20000			Xiao *et al.*[184]
Self-assembly graphene organogel		140		2			Sun *et al.*[185]
3-D graphene foam network	850			10			Yavari *et al.*[187]

The chemically reduced giant graphene fibers from calcium chloride coagulation possessed an electrical conductivity of 41 200 S·m^{-1}.[143] However, the highest conductivity to date results from a chemically assembled graphene structure bearing an N-doped graphene hierarchical ordered system at 64 900 S·m^{-1}.[127]

OPPORTUNITIES AND OUTLOOK

Graphenes possess useful properties by virtue of their single layer, which distinguishes them from multilayer graphene or graphite systems. Single layer graphene, graphene oxide and few-layer graphene oxide exhibit flexibility in their lattice, allowing the sheets to contort and conform to nonplanar architecture. The changes in the architecture of graphene induce lattice curvature and bond strain, which directly affect its conductive properties. Moreover, the sheet morphology can also better interface with other graphene sheets or host matrices, thus extending the conductive properties over longer ranges and improving graphene—graphene or graphene—host interactions to increase its mechanical performance. Graphene oxide, by virtue of its oxygen containing groups and lattice defects, is more susceptible to structural

changes whether through direct or indirect influence of its chemical environment. Several key chemical methods in which to bring about changes in graphene and graphene oxide architecture are highlighted.

Among the most important graphene sheet chemistry affecting morphology are the reactions that lead to hierarchical structures, where the desired unit cell is repeated, thus ensuring a homogeneous rather than localized performance. These systems have been developed based on the more readily available graphene oxide starting material, where the reaction can involve reduction of the oxygen-containing groups to generate conductive systems that also exhibit excellent mechanical performance, high surface areas and high sorptive capacities. The chemically driven structural changes to graphene oxide have been shown to occur in solution, though is exacerbated to a limited extend on drying from a solvent. When coupled with its ability to undergo nonsolution chemical reduction (*e.g.*, hydrazine vapor), the architecture of the graphene system can be preserved from the initial reactions or extended further with subsequent reactions (*e.g.*, polycondensation). Furthermore, the incomplete chemical reduction of graphene oxide, while improving its conductivity, still presents a number of oxygen-containing groups available for additional functionalization (*e.g.*, biomolecule attachment to three-dimensional graphene systems).

Knowledge of graphene sheet chemistry affecting architecture provides invaluable insight toward large-scale preparation and control in the design of three-dimensional graphene-based systems with desired mechanical, thermal, electrical and/or chemical properties. This will lead to exciting systems that have the potential to be advance flexible displays, batteries, solar cells, medical devices, gas or liquid sorbents, and supercapacitors.

Conflict of Interest: The authors declare no competing financial interest.

Acknowledgment. This paper is dedicated to Professor Sir Harold Kroto F.R.S. in celebration of his 75th birthday. The Marie-Curie Industry-Academia Partnerships and Pathways programme (FP7-PEOPLE-IRSES-269267-ENSOR) is gratefully acknowledged.

REFERENCES AND NOTES

1. Novoselov, K. S.; Geim, A. K.; Morozov, S. V.; Jiang, D.; Zhang, Y.; Dubonos, S. V.; Grigorieva, I. V.; Firsov, A. A. Electric Field Effect in Atomically Thin Carbon Films. *Science* **2004**, *306*, 666–669.
2. Novoselov, K. S.; Jiang, Z.; Zhang, Y.; Morozov, S. V.; Stormer, H. L.; Zeitler, U.; Maan, J. C.; Boebinger, G. S.; Kim, P.; Geim, A. K. Room-Temperature Quantum Hall Effect in Graphene. *Science* **2007**, *315*, 1379–1379.
3. Meyer, J. C.; Geim, A. K.; Katsnelson, M. I.; Novoselov, K. S.; Booth, T. J.; Roth, S. The Structure of Suspended Graphene Sheets. *Nature* **2007**, *446*, 60–63.
4. Aristov, V. Y.; Urbanik, G.; Kummer, K.; Vyalikh, D. V.; Molodtsova, O. V.; Preobrajenski, A. B.; Zakharov, A. A.; Hess, C.; Haenke, T.; Buechner, B.; Vobornik, I.; Fujii, J.; Panaccione, G.; Ossipyan, Y. A.; Knupfer, M. Graphene Synthesis on Cubic SiC/Si Wafers. Perspectives for Mass Production of Graphene-Based Electronic Devices. *Nano Lett.* **2010**, *10*, 992–995.
5. Carlsson, J. M. Buckle or Break. *Nat. Mater.* **2007**, *6*, 801–802.
6. Fasolino, A.; Los, J. H.; Katsnelson, M. I. Intrinsic Ripples in Graphene. *Nat. Mater.* **2007**, *6*, 858–861.
7. Qiu, L.; Zhang, X.; Yang, W.; Wang, Y.; Simon, G. P.; Li, D. Controllable Corrugation of Chemically Converted Graphene Sheets in Water and Potential Application for Nanofiltration. *Chem. Commun.* **2011**, *47*, 5810–5812.
8. Srinivas, G.; Burress, J. W.; Ford, J.; Yildirim, T. Porous Graphene Oxide Frameworks: Synthesis and Gas Sorption Properties. *J. Mater. Chem.* **2011**, *21*, 11323–11329.
9. Burress, J. W.; Gadipelli, S.; Ford, J.; Simmons, J. M.; Zhou, W.; Yildirim, T. Graphene Oxide Framework Materials: Theoretical Predictions and Experimental Results. *Angew. Chem., Int. Ed.* **2010**, *49*, 8902–8904.
10. Jahan, M.; Bao, Q. L.; Loh, K. P. Electrocatalytically Active Graphene-Porphyrin Mof Composite for Oxygen Reduction Reaction. *J. Am. Chem. Soc.* **2012**, *134*, 6707–6713.
11. Lee, C.; Wei, X.; Kysar, J. W.; Hone, J. Measurement of the Elastic Properties and Intrinsic Strength of Monolayer Graphene. *Science* **2008**, *321*, 385–388.
12. Suk, J. W.; Piner, R. D.; An, J.; Ruoff, R. S. Mechanical Properties of Mono Layer Graphene Oxide. *ACS Nano* **2010**, *4*, 6557–6564.
13. Baringhaus, J.; Ruan, M.; Edler, F.; Tejeda, A.; Sicot, M.; Taleb-Ibrahimi, A.; Li, A.-P.; Jiang, Z.; Conrad, E. H.; Berger, C.; Tegenkamp, C.; de Heer, W. A. Exceptional Ballistic Transport in Epitaxial Graphene Nanoribbons. *Nature* **2014**, *506*, 349–354.
14. Zhu, Y.; Murali, S.; Cai, W.; Li, X.; Suk, J. W.; Potts, J. R.; Ruoff, R. S. Graphene and Graphene Oxide: Synthesis, Properties, and Applications. *Adv. Mater.* **2010**, *22*, 3906–3924.
15. Li, C.; Shi, G. Three-Dimensional Graphene Architectures. *Nanoscale* **2012**, *4*, 5549–5563.
16. Locatelli, A.; Wang, C.; Africh, C.; Stojic, N.; Mentes, T. O.; Comelli, G.; Binggeli, N. Temperature-Driven Reversible Rippling and Bonding of a Graphene Super Lattice. *ACS Nano* **2013**, *7*, 6955–6963.
17. Sutter, P.; Hybertsen, M. S.; Sadowski, J. T.; Sutter, E. Electronic Structure of Few-Layer Epitaxial Graphene on Ru(0001). *Nano Lett.* **2009**, *9*, 2654–2660.
18. Schniepp, H. C.; Li, J. L.; McAllister, M. J.; Sai, H.; Herrera-Alonso, M.; Adamson, D. H.; Prud'homme, R. K.; Car, R.; Saville, D. A.; Aksay, I. A. Functionalized Single Graphene Sheets Derived from Splitting Graphite Oxide. *J. Phys. Chem. B* **2006**, *110*, 8535–8539.
19. Valles, C.; Nunez, J. D.; Benito, A. M.; Maser, W. K. Flexible Conductive Graphene Paper Obtained by Direct and Gentle Annealing of Graphene Oxide Paper. *Carbon* **2012**, *50*, 835–844.
20. Dikin, D. A.; Stankovich, S.; Zimney, E. J.; Piner, R. D.; Dommett, G. H. B.; Evmenenko, G.; Nguyen, S. T.; Ruoff, R. S. Preparation and Characterization of Graphene Oxide Paper. *Nature* **2007**, *448*, 457–460.
21. Ansari, S.; Giannelis, E. P. Functionalized Graphene Sheet-Poly(vinylidene fluoride) Conductive Nanocomposites. *J. Polym. Sci., Part B: Polym. Phys.* **2009**, *47*, 888–897.
22. Roldughin, V. I.; Vysotskii, V. V. Percolation Properties of Metal-Filled Polymer Films, Structure and Mechanisms of Conductivity. *Prog. Org. Coat.* **2000**, *39*, 81–100.
23. Hicks, J.; Behnam, A.; Ural, A. A Computational Study of Tunneling-Percolation Electrical Transport in Graphene-Based Nanocomposites. *Appl. Phys. Lett.* **2009**, *95*.
24. Qiu, L.; Liu, D.; Wang, Y.; Cheng, C.; Zhou, K.; Ding, J.; Van-Tan, T.; Li, D. Mechanically Robust, Electrically Conductive and Stimuli-Responsive Binary Network Hydrogels Enabled by Superelastic Graphene Aerogels. *Adv. Mater.* **2014**, *26*, 3333–3337.
25. Bao, W. S.; Meguid, S. A.; Zhu, Z. H.; Meguid, M. J. Modeling Electrical Conductivities of Nanocomposites with Aligned Carbon Nanotubes. *Nanotechnology* **2011**, *22*, No. 485704.
26. Schiffres, S. N.; Harish, S.; Maruyama, S.; Shiomi, J.; Malen, J. A. Tunable Electrical and Thermal Transport in

Ice-Templated Multi Layer Graphene Nanocomposites through Freezing Rate Control. *ACS Nano* **2013**, *7*, 11183–11189.
27. Kim, H.; Macosko, C. W. Processing-Property Relationships of Polycarbonate/Graphene Composites. *Polymer* **2009**, *50*, 3797–3809.
28. Kim, K.; Lee, Z.; Malone, B. D.; Chan, K. T.; Aleman, B.; Regan, W.; Gannett, W.; Crommie, M. F.; Cohen, M. L.; Zettl, A. Multiply Folded Graphene. *Phys. Rev. B* **2011**, *83*, No. 245433.
29. Gao, J.; Bai, H.; Zhou, X.; Yang, G.; Xu, C.; Zhang, Q.; Chen, F.; Fu, Q. Observation of Strong Nano-Effect *via* Tuning Distributed Architecture of Graphene Oxide in Poly(propylene carbonate). *Nanotechnology* **2014**, *25*, No. 025702.
30. Potschke, P.; Paul, D. R. Formation of Co-Continuous Structures in Melt-Mixed Immiscible Polymer Blends. *J. Macromol. Sci. Polym. Rev.* **2003**, *C43*, 87–141.
31. Gutierrez, M. C.; Garcia-Carvajal, Z. Y.; Jobbagy, M.; Rubio, T.; Yuste, L.; Rojo, F.; Ferrer, M. L.; del Monte, F. Poly(vinyl alcohol) Scaffolds with Tailored Morphologies for Drug Delivery and Controlled Release. *Adv. Funct. Mater.* **2007**, *17*, 3505–3513.
32. Choi, W.; Lahiri, I.; Seelaboyina, R.; Kang, Y. S. Synthesis of Graphene and Its Applications: A Review. *Crit. Rev. Solid State Mater.* **2010**, *35*, 52–71.
33. Dreyer, D. R.; Park, S.; Bielawski, C. W.; Ruoff, R. S. The Chemistry of Graphene Oxide. *Chem. Soc. Rev.* **2010**, *39*, 228–240.
34. Eda, G.; Chhowalla, M. Chemically Derived Graphene Oxide: Towards Large-Area Thin-Film Electronics and Optoelectronics. *Adv. Mater.* **2010**, *22*, 2392–2415.
35. Huang, X.; Yin, Z.; Wu, S.; Qi, X.; He, Q.; Zhang, Q.; Yan, Q.; Boey, F.; Zhang, H. Graphene-Based Materials: Synthesis, Characterization, Properties, and Applications. *Small* **2011**, *7*, 1876–1902.
36. Singh, V.; Joung, D.; Zhai, L.; Das, S.; Khondaker, S. I.; Seal, S. Graphene Based Materials: Past, Present and Future. *Prog. Mater. Sci.* **2011**, *56*, 1178–1271.
37. Wang, H.; Maiyalagan, T.; Wang, X. Review on Recent Progress in Nitrogen-Doped Graphene: Synthesis, Characterization, and Its Potential Applications. *ACS Catal.* **2012**, *2*, 781–794.
38. Saito, K.; Nakamura, J.; Natori, A. Ballistic Thermal Conductance of a Graphene Sheet. *Phys. Rev. B* **2007**, *76*, No. 115409.
39. Geim, A. K.; Novoselov, K. S. The Rise of Graphene. *Nat. Mater.* **2007**, *6*, 183–191.
40. Li, D.; Kaner, R. B. Materials Science—Graphene-Based Materials. *Science* **2008**, *320*, 1170–1171.
41. Wu, Q.; Xu, Y.; Yao, Z.; Liu, A.; Shi, G. Supercapacitors Based on Flexible Graphene/Polyaniline Nanofiber Composite Films. *ACS Nano* **2010**, *4*, 1963–1970.
42. Yang, X.; Zhu, J.; Qiu, L.; Li, D. Bioinspired Effective Prevention of Restacking in Multilayered Graphene Films: Towards the Next Generation of High-Performance Supercapacitors. *Adv. Mater.* **2011**, *23*, 2833–2838.
43. Yang, X.; Cheng, C.; Wang, Y.; Qiu, L.; Li, D. Liquid-Mediated Dense Integration of Graphene Materials for Compact Capacitive Energy Storage. *Science* **2013**, *341*, 534–537.
44. Ohta, T.; Bostwick, A.; McChesney, J. L.; Seyller, T.; Horn, K.; Rotenberg, E. Interlayer Interaction and Electronic Screening in Multilayer Graphene Investigated with Angle-Resolved Photoemission Spectroscopy. *Phys. Rev. Lett.* **2007**, *98*, No. 206802.
45. Pletikosic, I.; Kralj, M.; Pervan, P.; Brako, R.; Coraux, J.; N'Diaye, A. T.; Busse, C.; Michely, T. Dirac Cones and Minigaps for Graphene on Ir(111). *Phys. Rev. Lett.* **2009**, *102*, No. 056808.
46. Lee, J. H.; Shin, D. W.; Makotchenko, V. G.; Nazarov, A. S.; Fedorov, V. E.; Kim, Y. H.; Choi, J. Y.; Kim, J. M.; Yoo, J. B. One-Step Exfoliation Synthesis of Easily Soluble Graphite and Transparent Conducting Graphene Sheets. *Adv. Mater.* **2009**, *21*, 4383–4387.
47. Nuvoli, D.; Valentini, L.; Alzari, V.; Scognamillo, S.; Bon, S. B.; Piccinini, M.; Illescas, J.; Mariani, A. High Concentration Few-Layer Graphene Sheets Obtained by Liquid Phase Exfoliation of Graphite in Ionic Liquid. *J. Mater. Chem.* **2011**, *21*, 3428–3431.
48. Wang, X.; Fulvio, P. F.; Baker, G. A.; Veith, G. M.; Unocic, R. R.; Mahurin, S. M.; Chi, M.; Dai, S. Direct Exfoliation of Natural Graphite into Micrometre Size Few Layers Graphene Sheets Using Ionic Liquids. *Chem. Commun.* **2010**, *46*, 4487–4489.
49. Park, K. H.; Kim, B. H.; Song, S. H.; Kwon, J.; Kong, B. S.; Kang, K.; Jeon, S. Exfoliation of Non-Oxidized Graphene Flakes for Scalable Conductive Film. *Nano Lett.* **2012**, *12*, 2871–2876.
50. Malik, S.; Vijayaraghavan, A.; Erni, R.; Ariga, K.; Khalakhan, I.; Hill, J. P. High Purity Graphenes Prepared by a Chemical Intercalation Method. *Nanoscale* **2010**, *2*, 2139–2143.
51. Green, A. A.; Hersam, M. C. Solution Phase Production of Graphene with Controlled Thickness *via* Density Differentiation. *Nano Lett.* **2009**, *9*, 4031–4036.
52. Byun, S.-J.; Lim, H.; Shin, G.-Y.; Han, T.-H.; Oh, S. H.; Ahn, J.-H.; Choi, H. C.; Lee, T.-W. Graphenes Converted from Polymers. *J. Phys. Chem. Lett.* **2011**, *2*, 493–497.
53. Korobeinyk, A. V.; Whitby, R. L. D.; Salvage, J. P.; Mikhalovsky, S. V. Exfoliated Production of Single- and Multi-Layer Graphenes and Carbon Nanofibres from the Carbonisation of a Co-Polymer. *Carbon* **2012**, *50*, 2018–2025.
54. Hummers, W. S.; Offeman, R. E. Preparation of Graphitic Oxide. *J. Am. Chem. Soc.* **1958**, *80*, 1339–1339.
55. Shao, G.; Lu, Y.; Wu, F.; Yang, C.; Zeng, F.; Wu, Q. Graphene Oxide: The Mechanisms of Oxidation and Exfoliation. *J. Mater. Sci.* **2012**, *47*, 4400–4409.
56. Li, D.; Muller, M. B.; Gilje, S.; Kaner, R. B.; Wallace, G. G. Processable Aqueous Dispersions of Graphene Nanosheets. *Nat. Nanotechnol.* **2008**, *3*, 101–105.
57. Stankovich, S.; Dikin, D. A.; Piner, R. D.; Kohlhaas, K. A.; Kleinhammes, A.; Jia, Y.; Wu, Y.; Nguyen, S. T.; Ruoff, R. S. Synthesis of Graphene-Based Nanosheets *via* Chemical Reduction of Exfoliated Graphite Oxide. *Carbon* **2007**, *45*, 1558–1565.
58. Shin, H.-J.; Kim, K. K.; Benayad, A.; Yoon, S.-M.; Park, H. K.; Jung, I.-S.; Jin, M. H.; Jeong, H.-K.; Kim, J. M.; Choi, J.-Y.; Lee, Y. H. Efficient Reduction of Graphite Oxide by Sodium Borohydride and Its Effect on Electrical Conductance. *Adv. Funct. Mater.* **2009**, *19*, 1987–1992.
59. Wei, Z. Q.; Wang, D. B.; Kim, S.; Kim, S. Y.; Hu, Y. K.; Yakes, M. K.; Laracuente, A. R.; Dai, Z. T.; Marder, S. R.; Berger, C.; King, W. P.; de Heer, W. A.; Sheehan, P. E.; Riedo, E. Nanoscale Tunable Reduction of Graphene Oxide for Graphene Electronics. *Science* **2010**, *328*, 1373–1376.
60. Chen, W.; Yan, L.; Bangal, P. R. Preparation of Graphene by the Rapid and Mild Thermal Reduction of Graphene Oxide Induced by Microwaves. *Carbon* **2010**, *48*, 1146–1152.
61. Whitby, R. L. D.; Korobeinyk, A.; Glevatska, K. V. Morphological Changes and Covalent Reactivity Assessment of Single-Layer Graphene Oxides under Carboxylic Group-Targeted Chemistry. *Carbon* **2011**, *49*, 722–725.
62. Pei, S. F.; Cheng, H. M. The Reduction of Graphene Oxide. *Carbon* **2012**, *50*, 3210–3228.
63. Qiu, L.; Yang, X.; Gou, X.; Yang, W.; Ma, Z.-F.; Wallace, G. G.; Li, D. Dispersing Carbon Nanotubes with Graphene Oxide in Water and Synergistic Effects between Graphene Derivatives. *Chem.—Eur. J.* **2010**, *16*, 10653–10658.
64. Rinzler, A. G.; Liu, J.; Dai, H.; Nikolaev, P.; Huffman, C. B.; Rodriguez-Macias, F. J.; Boul, P. J.; Lu, A. H.; Heymann, D.; Colbert, D. T.; Lee, R. S.; Fischer, J. E.; Rao, A. M.; Eklund, P. C.; Smalley, R. E. Large-Scale Purification of Single-Wall Carbon Nanotubes: Process, Product, and Characterization. *Appl. Phys. A Mater.* **1998**, *67*, 29–37.
65. Wang, Z. W.; Shirley, M. D.; Meikle, S. T.; Whitby, R. L. D.; Mikhalovsky, S. V. The Surface Acidity of Acid Oxidised Multi-Walled Carbon Nanotubes and the Influence of

in Situ Generated Fulvic Acids on Their Stability in Aqueous Dispersions. *Carbon* **2009**, *47*, 73–79.
66. Salzmann, C. G.; Llewellyn, S. A.; Tobias, G.; Ward, M. A. H.; Huh, Y.; Green, M. L. H. The Role of Carboxylated Carbonaceous Fragments in the Functionalization and Spectroscopy of a Single-Walled Carbon-Nanotube Material. *Adv. Mater.* **2007**, *19*, 883–887.
67. Verdejo, R.; Lamoriniere, S.; Cottam, B.; Bismarck, A.; Shaffer, M. Removal of Oxidation Debris from Multi-Walled Carbon Nanotubes. *Chem. Commun.* **2007**, 513–515.
68. Rourke, J. P.; Pandey, P. A.; Moore, J. J.; Bates, M.; Kinloch, I. A.; Young, R. J.; Wilson, N. R. The Real Graphene Oxide Revealed: Stripping the Oxidative Debris from the Graphene-Like Sheets. *Angew. Chem., Int. Ed.* **2011**, *50*, 3173–3177.
69. Karabanova, L. V.; Whitby, R. L. D.; Korobeinyk, A.; Bondaruk, O.; Salvage, J. P.; Lloyd, A. W.; Mikhalovsky, S. V. Microstructure Changes of Polyurethane by Inclusion of Chemically Modified Carbon Nanotubes at Low Filler Contents. *Compos. Sci. Technol.* **2012**, *72*, 865–872.
70. He, H. Y.; Klinowski, J.; Forster, M.; Lerf, A. A New Structural Model for Graphite Oxide. *Chem. Phys. Lett.* **1998**, *287*, 53–56.
71. Lerf, A.; He, H. Y.; Forster, M.; Klinowski, J. Structure of Graphite Oxide Revisited. *J. Phys. Chem. B* **1998**, *102*, 4477–4482.
72. Park, S.; An, J.; Jung, I.; Piner, R. D.; An, S. J.; Li, X.; Velamakanni, A.; Ruoff, R. S. Colloidal Suspensions of Highly Reduced Graphene Oxide in a Wide Variety of Organic Solvents. *Nano Lett.* **2009**, *9*, 1593–1597.
73. Tao, C.-a.; Wang, J.; Qin, S.; Lv, Y.; Long, Y.; Zhu, H.; Jiang, Z. Fabrication of Ph-Sensitive Graphene Oxide-Drug Supramolecular Hydrogels as Controlled Release Systems. *J. Mater. Chem.* **2012**, *22*, 24856–24861.
74. Koenig, S. P.; Boddeti, N. G.; Dunn, M. L.; Bunch, J. S. Ultrastrong Adhesion of Graphene Membranes. *Nat. Nanotechnol.* **2011**, *6*, 543–546.
75. Schniepp, H. C.; Kudin, K. N.; Li, J.-L.; Prud'homme, R. K.; Car, R.; Saville, D. A.; Aksay, I. A. Bending Properties of Single Functionalized Graphene Sheets Probed by Atomic Force Microscopy. *ACS Nano* **2008**, *2*, 2577–2584.
76. Xu, Z.; Buehler, M. J. Geometry Controls Conformation of Graphene Sheets: Membranes, Ribbons, and Scrolls. *ACS Nano* **2010**, *4*, 3869–3876.
77. Shenoy, V. B.; Reddy, C. D.; Ramasubramaniam, A.; Zhang, Y. W. Edge-Stress-Induced Warping of Graphene Sheets and Nanoribbons. *Phys. Rev. Lett.* **2008**, *101*.
78. Meng, X.; Li, M.; Kang, Z.; Zhang, X.; Xiao, J. Mechanics of Self-Folding of Single-Layer Graphene. *J. Phys. D: Appl. Phys.* **2013**, *46*.
79. Patra, N.; Wang, B.; Kral, P. Nanodroplet Activated and Guided Folding of Graphene Nanostructures. *Nano Lett.* **2009**, *9*, 3766–3771.
80. Ham, H.; Van Khai, T.; Park, N.-H.; So, D. S.; Lee, J.-W.; Na, H. G.; Kwon, Y. J.; Cho, H. Y.; Kim, H. W. Freeze-Drying-Induced Changes in the Properties of Graphene Oxides. *Nanotechnology* **2014**, *25*, No. 235601.
81. Castro Neto, A. H.; Guinea, F.; Peres, N. M. R.; Novoselov, K. S.; Geim, A. K. The Electronic Properties of Graphene. *Rev. Mod. Phys.* **2009**, *81*, 109–162.
82. Liu, Z.; Suenaga, K.; Harris, P. J. F.; Iijima, S. Open and Closed Edges of Graphene Layers. *Phys. Rev. Lett.* **2009**, *102*.
83. Zhang, J.; Xiao, J.; Meng, X.; Monroe, C.; Huang, Y.; Zuo, J.-M. Free Folding of Suspended Graphene Sheets by Random Mechanical Stimulation. *Phys. Rev. Lett.* **2010**, *104*.
84. Roy, H. V.; Kallinger, C.; Sattler, K. Study of Single and Multiple Foldings of Graphitic Sheets. *Surf. Sci.* **1998**, *407*, 1–6.
85. Huang, J. Y.; Ding, F.; Yakobson, B. I.; Lu, P.; Qi, L.; Li, J. *In Situ* Observation of Graphene Sublimation and Multi-Layer Edge Reconstructions. *Proc. Natl. Acad. Sci. U.S.A.* **2009**, *106*, 10103–10108.
86. Prada, E.; San-Jose, P.; Brey, L. Zero Landau Level in Folded Graphene Nanoribbons. *Phys. Rev. Lett.* **2010**, *105*, No. 106802.
87. Rainis, D.; Taddei, F.; Polini, M.; Leon, G.; Guinea, F.; Fal'ko, V. I. Gauge Fields and Interferometry in Folded Graphene. *Phys. Rev. B* **2011**, *83*, No. 165403.
88. Park, S.; Srivastava, D.; Cho, K. Generalized Chemical Reactivity of Curved Surfaces: Carbon Nanotubes. *Nano Lett.* **2003**, *3*, 1273–1277.
89. Xie, X.; Ju, L.; Feng, X.; Sun, Y.; Zhou, R.; Liu, K.; Fan, S.; Li, Q.; Jiang, K. Controlled Fabrication of High-Quality Carbon Nanoscrolls from Monolayer Graphene. *Nano Lett.* **2009**, *9*, 2565–2570.
90. Smith, R. J.; Lotya, M.; Coleman, J. N. The Importance of Repulsive Potential Barriers for the Dispersion of Graphene Using Surfactants. *New J. Phys.* **2010**, *12*, No. 125008.
91. Sidorov, A.; Mudd, D.; Sumanasekera, G.; Ouseph, P. J.; Jayanthi, C. S.; Wu, S. Y. Electrostatic Deposition of Graphene in a Gaseous Environment: A Deterministic Route for Synthesizing Rolled Graphenes? *Nanotechnology* **2009**, *20*, 5.
92. Liu, H.; Li, S. H.; Zhai, J.; Li, H. J.; Zheng, Q. S.; Jiang, L.; Zhu, D. B. Self-Assembly of Large-Scale Micropatterns on Aligned Carbon Nanotube Films. *Angew. Chem., Int. Ed.* **2004**, *43*, 1146–1149.
93. Whitby, R. L. D.; Fukuda, T.; Maekawa, T.; James, S. L.; Mikhalovsky, S. V. Geometric Control and Tuneable Pore Size Distribution of Buckypaper and Buckydiscs. *Carbon* **2008**, *46*, 949–956.
94. Luo, J.; Jang, H. D.; Huang, J. Effect of Sheet Morphology on the Scalability of Graphene-Based Ultracapacitors. *ACS Nano* **2013**, *7*, 1464–1471.
95. Ausman, K. D.; Piner, R.; Lourie, O.; Ruoff, R. S.; Korobov, M. Organic Solvent Dispersions of Single-Walled Carbon Nanotubes: Toward Solutions of Pristine Nanotubes. *J. Phys. Chem. B* **2000**, *104*, 8911–8915.
96. Tang, Q. Y.; Shafiq, I.; Chan, Y. C.; Wong, N. B.; Cheung, R. Study of the Dispersion and Electrical Properties of Carbon Nanotubes Treated by Surfactants in Dimethylacetamide. *J. Nanosci. Nanotechnol.* **2010**, *10*, 4967–4974.
97. Ryu, S.; Lee, B.; Hong, S.; Jin, S.; Park, S.; Hong, S. H.; Lee, H. Salting-out as a Scalable, in-Series Purification Method of Graphene Oxides from Microsheets to Quantum Dots. *Carbon* **2013**, *63*, 45–53.
98. Boehm, H. P. Some Aspects of the Surface Chemistry of Carbon Blacks and Other Carbons. *Carbon* **1994**, *32*, 759–769.
99. Yang, D.; Velamakanni, A.; Bozoklu, G.; Park, S.; Stoller, M.; Piner, R. D.; Stankovich, S.; Jung, I.; Field, D. A.; Ventrice, C. A., Jr.; Ruoff, R. S. Chemical Analysis of Graphene Oxide Films after Heat and Chemical Treatments by X-Ray Photoelectron and Micro-Raman Spectroscopy. *Carbon* **2009**, *47*, 145–152.
100. Laszlo, K.; Josepovits, K.; Tombacz, E. Analysis of Active Sites on Synthetic Carbon Surfaces by Various Methods. *Anal. Sci.* **2001**, *17*, i1741–i1744.
101. Loh, K. P.; Bao, Q.; Eda, G.; Chhowalla, M. Graphene Oxide as a Chemically Tunable Platform for Optical Applications. *Nat. Chem.* **2010**, *2*, 1015–1024.
102. Whitby, R. L. D.; Korobeinyk, A.; Gun'ko, V. M.; Busquets, R.; Cundy, A. B.; Laszlo, K.; Skubiszewska-Zieba, J.; Leboda, R.; Tombacz, E.; Toth, I. Y.; Kovacs, K.; Mikhalovsky, S. V. Ph-Driven Physicochemical Conformational Changes of Single-Layer Graphene Oxide. *Chem. Commun.* **2011**, *47*, 9645–9647.
103. Whitby, R. L. D.; Gun'ko, V. M.; Korobeinyk, A.; Busquets, R.; Cundy, A. B.; Laszlo, K.; Skubiszewska-Zieba, J.; Leboda, R.; Tombacz, E.; Toth, I. Y.; Kovacs, K.; Mikhalovsky, S. V. Driving Forces of Conformational Changes in Single-Layer Graphene Oxide. *ACS Nano* **2012**, *6*, 3967–3973.
104. Vickery, J. L.; Patil, A. J.; Mann, S. Fabrication of Graphene-Polymer Nanocomposites with Higher-Order Three-Dimensional Architectures. *Adv. Mater.* **2009**, *21*, 2180–2184.

105. Zu, S.-Z.; Han, B.-H. Aqueous Dispersion of Graphene Sheets Stabilized by Pluronic Copolymers: Formation of Supramolecular Hydrogel. *J. Phys. Chem. C* **2009**, *113*, 13651–13657.
106. Chen, Z.; Ren, W.; Gao, L.; Liu, B.; Pei, S.; Cheng, H.-M. Three-Dimensional Flexible and Conductive Interconnected Graphene Networks Grown by Chemical Vapour Deposition. *Nat. Mater.* **2011**, *10*, 424–428.
107. Chen, Y.; Guo, F.; Jachak, A.; Kim, S.-P.; Datta, D.; Liu, J.; Kulaots, I.; Vaslet, C.; Jang, H. D.; Huang, J.; Kane, A.; Shenoy, V. B.; Hurt, R. H. Aerosol Synthesis of Cargo-Filled Graphene Nanosacks. *Nano Lett.* **2012**, *12*, 1996–2002.
108. Dappe, Y. J.; Basanta, M. A.; Flores, F.; Ortega, J. Weak Chemical Interaction and Van Der Waals Forces between Graphene Layers: A Combined Density Functional and Intermolecular Perturbation Theory Approach. *Phys. Rev. B* **2006**, *74*.
109. Woltornist, S. J.; Oyer, A. J.; Carrillo, J.-M. Y.; Dobrynin, A. V.; Adamson, D. H. Conductive Thin Films of Pristine Graphene by Solvent Interface Trapping. *ACS Nano* **2013**, *7*, 7062–7066.
110. Noel, A.; Faucheu, J.; Rieu, M.; Viricelle, J.-P.; Bourgeat-Lami, E. Tunable Architecture for Flexible and Highly Conductive Graphene-Polymer Composites. *Compos. Sci. Technol.* **2014**, *95*, 82–88.
111. Choi, B. G.; Yang, M.; Hong, W. H.; Choi, J. W.; Huh, Y. S. 3D Macroporous Graphene Frameworks for Supercapacitors with High Energy and Power Densities. *ACS Nano* **2012**, *6*, 4020–4028.
112. Sohn, K.; Na, Y. J.; Chang, H.; Roh, K.-M.; Jang, H. D.; Huang, J. Oil Absorbing Graphene Capsules by Capillary Molding. *Chem. Commun.* **2012**, *48*, 5968–5970.
113. Wang, H.; Zhang, D.; Yan, T.; Wen, X.; Zhang, J.; Shi, L.; Zhong, Q. Three-Dimensional Macroporous Graphene Architectures as High Performance Electrodes for Capacitive Deionization. *J. Mater. Chem. A* **2013**, *1*, 11778–11789.
114. Zhou, D.; Han, B.-H. Graphene-Based Nanoporous Materials Assembled by Mediation of Polyoxometalate Nanoparticles. *Adv. Funct. Mater.* **2010**, *20*, 2717–2722.
115. Wong, L. L. C.; Barg, S.; Menner, A.; Pereira, P. d. V.; Eda, G.; Chowalla, M.; Saiz, E.; Bismarck, A. Macroporous Polymer Nanocomposites Synthesised from High Internal Phase Emulsion Templates Stabilised by Reduced Graphene Oxide. *Polymer* **2014**, *55*, 395–402.
116. Ma, H.; Gao, P.; Fan, D.; Du, B.; Hao, J.; Wei, Q. Assembly of Graphene Nanocomposites into Honeycomb-Structured Macroporous Films with Enhanced Hydrophobicity. *New. J. Chem.* **2013**, *37*, 1307–1311.
117. Chen, D.; Ji, G.; Ma, Y.; Lee, J. Y.; Lu, J. Graphene-Encapsulated Hollow Fe3O4 Nanoparticle Aggregates as a High-Performance Anode Material for Lithium Ion Batteries. *ACS Appl. Mater. Interfaces* **2011**, *3*, 3078–3083.
118. Zhang, F.; Zhu, D.; Chen, X. a.; Xu, X.; Yang, Z.; Zou, C.; Yang, K.; Huang, S. A Nickel Hydroxide-Coated 3D Porous Graphene Hollow Sphere Framework as a High Performance Electrode Material for Supercapacitors. *Phys. Chem. Chem. Phys.* **2014**, *16*, 4186–4192.
119. Kim, J. H.; Lee, S.; Lee, J. W.; Song, T.; Paik, U. 3d-Interconnected Nanoporous Rgo-Cnt Structure for Supercapacitors Application. *Electrochim. Acta* **2014**, *125*, 536–542.
120. Jang, H. D.; Kim, S. K.; Chang, H.; Roh, K.-M.; Choi, J.-W.; Huang, J. A Glucose Biosensor Based on TiO_2-Graphene Composite. *Biosens. Bioelectron.* **2012**, *38*, 184–188.
121. Yan, W.; He, F.; Gai, S.; Gao, P.; Chen, Y.; Yang, P. A Novel 3d Structured Reduced Graphene Oxide/TiO_2 Composite: Synthesis and Photocatalytic Performance. *J. Mater. Chem. A* **2014**, *2*, 3605–3612.
122. Gu, Y.; Wu, H.; Xiong, Z.; Al Abdulla, W.; Zhao, X. S. The Electrocapacitive Properties of Hierarchical Porous Reduced Graphene Oxide Templated by Hydrophobic CaCO3 Spheres. *J. Mater. Chem. A* **2014**, *2*, 451–459.
123. Qin, J.; He, C.; Zhao, N.; Wang, Z.; Shi, C.; Liu, E.-Z.; Li, J. Graphene Networks Anchored with Sn@Graphene as Lithium Ion Battery Anode. *ACS Nano* **2014**, *8*, 1728–1738.
124. Zhou, X.; Liu, W.; Yu, X.; Liu, Y.; Fang, Y.; Klankowski, S.; Yang, Y.; Brown, J. E.; Li, J. Tin Dioxide@Carbon Core-Shell Nanoarchitectures Anchored on Wrinkled Graphene for Ultrafast and Stable Lithium Storage. *ACS Appl. Mater. Interfaces* **2014**, *6*, 7434–7443.
125. Gong, Y.; Meng, X.; Zou, C.; Yao, Y.; Fu, W.; Wang, M.; Yin, G.; Huang, Z.; Liao, X.; Chen, X. A Facile One-Pot Synthesis of Yolk-Shell ZnO Microsphere-Graphene Composite Induced by Graphene Oxide. *Mater. Lett.* **2013**, *106*, 171–174.
126. Shi, Y.; Wang, J.-Z.; Chou, S.-L.; Wexler, D.; Li, H.-J.; Ozawa, K.; Liu, H.-K.; Wu, Y.-P. Hollow Structured Li3vo4 Wrapped with Graphene Nanosheets *in Situ* Prepared by a One-Pot Template-Free Method as an Anode for Lithium-Ion Batteries. *Nano Lett.* **2013**, *13*, 4715–4720.
127. Lee, S. H.; Kim, H. W.; Hwang, J. O.; Lee, W. J.; Kwon, J.; Bielawski, C. W.; Ruoff, R. S.; Kim, S. O. Three-Dimensional Self-Assembly of Graphene Oxide Platelets into Mechanically Flexible Macroporous Carbon Films. *Angew. Chem., Int. Ed.* **2010**, *49*, 10084–10088.
128. Niu, T.; Liu, G. L.; Liu, Y. Preparation of Ru/Graphene-Meso-Macroporous SiO2 Composite and Their Application to the Preferential Oxidation of Co in H-2-Rich Gases. *Appl. Catal., B* **2014**, *154*, 82–92.
129. Wu, C.; Huang, X.; Wu, X.; Qian, R.; Jiang, P. Mechanically Flexible and Multifunctional Polymer-Based Graphene Foams for Elastic Conductors and Oil-Water Separators. *Adv. Mater.* **2013**, *25*, 5658–5662.
130. Wilson, P. M.; Mbah, G. N.; Smith, T. G.; Schmidt, D.; Lai, R. Y.; Hofmann, T.; Sinitskii, A. Three-Dimensional Periodic Graphene Nanostructures. *J. Mater. Chem. C* **2014**, *2*, 1879–1886.
131. Xiao, X.; Beechem, T. E.; Brumbach, M. T.; Lambert, T. N.; Davis, D. J.; Michael, J. R.; Washburn, C. M.; Wang, J.; Brozik, S. M.; Wheeler, D. R.; Burckel, D. B.; Polsky, R. Lithographically Defined Three-Dimensional Graphene Structures. *ACS Nano* **2012**, *6*, 3573–3579.
132. Meng, Y.; Wang, K.; Zhang, Y.; Wei, Z. Hierarchical Porous Graphene/Polyaniline Composite Film with Superior Rate Performance for Flexible Supercapacitors. *Adv. Mater.* **2013**, *25*, 6985–6990.
133. Bai, H.; Li, C.; Wang, X.; Shi, G. A Ph-Sensitive Graphene Oxide Composite Hydrogel. *Chem. Commun.* **2010**, *46*, 2376–2378.
134. Bai, H.; Li, C.; Wang, X.; Shi, G. On the Gelation of Graphene Oxide. *J. Phys. Chem. C* **2011**, *115*, 5545–5551.
135. Compton, O. C.; An, Z.; Putz, K. W.; Hong, B. J.; Hauser, B. G.; Brinson, L. C.; Nguyen, S. T. Additive-Free Hydrogelation of Graphene Oxide by Ultrasonication. *Carbon* **2012**, *50*, 3399–3406.
136. Yun, S.; Kang, S.-O.; Park, S.; Park, H. S. CO_2-Activated, Hierarchical Trimodal Porous Graphene Frameworks for Ultrahigh and Ultrafast Capacitive Behavior. *Nanoscale* **2014**, *6*, 5296–5302.
137. Chang, Y.; Li, J.; Wang, B.; Luo, H.; He, H.; Song, Q.; Zhi, L. Synthesis of 3d Nitrogen-Doped Graphene/Fe_3O_4 by a Metal Ion Induced Self-Assembly Process for High-Performance Li-Ion Batteries. *J. Mater. Chem. A* **2013**, *1*, 14658–14665.
138. Xu, Y.; Sheng, K.; Li, C.; Shi, G. Self-Assembled Graphene Hydrogel *via* a One-Step Hydrothermal Process. *ACS Nano* **2010**, *4*, 4324–4330.
139. Niu, Z.; Chen, J.; Hng, H. H.; Ma, J.; Chen, X. A Leavening Strategy to Prepare Reduced Graphene Oxide Foams. *Adv. Mater.* **2012**, *24*, 4144–4150.
140. Bi, H.; Xie, X.; Yin, K.; Zhou, Y.; Wan, S.; Ruoff, R. S.; Sun, L. Highly Enhanced Performance of Spongy Graphene as an Oil Sorbent. *J. Mater. Chem. A* **2014**, *2*, 1652–1656.
141. Yu, S. X.; Yang, L. W.; Tian, Y.; Yang, P.; Jiang, F.; Hu, S. W.; Wei, X. L.; Zhong, J. X. Mesoporous Anatase TiO_2 Submicrospheres Embedded in Self-Assembled Three-Dimensional Reduced Graphene Oxide Networks for Enhanced Lithium Storage. *J. Mater. Chem. A* **2013**, *1*, 12750–12758.
142. Sheng, K.; Sun, Y.; Li, C.; Yuan, W.; Shi, G. Ultrahigh-Rate Supercapacitors Based on Eletrochemically Reduced Graphene Oxide for Ac Line-Filtering. *Sci. Rep.* **2012**, *2*.

143. Xu, Z.; Sun, H.; Zhao, X.; Gao, C. Ultrastrong Fibers Assembled from Giant Graphene Oxide Sheets. *Adv. Mater.* **2013**, *25*, 188–193.
144. Xu, Z.; Zhang, Y.; Li, P.; Gao, C. Strong, Conductive, Lightweight, Neat Graphene Aerogel Fibers with Aligned Pores. *ACS Nano* **2012**, *6*, 7103–7113.
145. Zhu, Y.; Murali, S.; Stoller, M. D.; Ganesh, K. J.; Cai, W.; Ferreira, P. J.; Pirkle, A.; Wallace, R. M.; Cychosz, K. A.; Thommes, M.; Su, D.; Stach, E. A.; Ruoff, R. S. Carbon-Based Supercapacitors Produced by Activation of Graphene. *Science* **2011**, *332*, 1537–1541.
146. Zhang, L. L.; Zhao, X.; Stoller, M. D.; Zhu, Y.; Ji, H.; Murali, S.; Wu, Y.; Perales, S.; Clevenger, B.; Ruoff, R. S. Highly Conductive and Porous Activated Reduced Graphene Oxide Films for High-Power Supercapacitors. *Nano Lett.* **2012**, *12*, 1806–1812.
147. Zhang, L.; Zhang, F.; Yang, X.; Long, G.; Wu, Y.; Zhang, T.; Leng, K.; Huang, Y.; Ma, Y.; Yu, A.; Chen, Y. Porous 3d Graphene-Based Bulk Materials with Exceptional High Surface Area and Excellent Conductivity for Supercapacitors. *Sci. Rep.* **2013**, *3*.
148. Liu, N.; Shen, J.; Liu, D. Activated High Specific Surface Area Carbon Aerogels for EDLCs. *Microporous Mesoporous Mater.* **2013**, *167*, 176–181.
149. Koh, K.; Wong-Foy, A. G.; Matzger, A. J. A Porous Coordination Copolymer with over 5000 M(2)/G Bet Surface Area. *J. Am. Chem. Soc.* **2009**, *131*, 4184–4185.
150. Loh, K. P.; Bao, Q.; Ang, P. K.; Yang, J. The Chemistry of Graphene. *J. Mater. Chem.* **2010**, *20*, 2277–2289.
151. Sun, Z.; James, D. K.; Tour, J. M. Graphene Chemistry: Synthesis and Manipulation. *J. Phys. Chem. Lett.* **2011**, *2*, 2425–2432.
152. Niyogi, S.; Bekyarova, E.; Hong, J.; Khizroev, S.; Berger, C.; de Heer, W.; Haddon, R. C. Covalent Chemistry for Graphene Electronics. *J. Phys. Chem. Lett.* **2011**, *2*, 2487–2498.
153. Chen, L.; Hu, H.; Ouyang, Y.; Pan, H. Z.; Sun, Y. Y.; Liu, F. Atomic Chemisorption on Graphene with Stone-Thrower-Wales Defects. *Carbon* **2011**, *49*, 3356–3361.
154. Liu, T. H.; Pao, C. W.; Chang, C. C. Effects of Dislocation Densities and Distributions on Graphene Grain Boundary Failure Strengths from Atomistic Simulations. *Carbon* **2012**, *50*, 3465–3472.
155. Chua, C. K.; Pumera, M. Chemical Reduction of Graphene Oxide: A Synthetic Chemistry Viewpoint. *Chem. Soc. Rev.* **2014**, *43*, 291–312.
156. Whitby, R. L. D.; Korobeinyk, A.; Mikhalovsky, S. V.; Fukuda, T.; Maekawa, T. Morphological Effects of Single-Layer Graphene Oxide in the Formation of Covalently Bonded Polypyrrole Composites Using Intermediate Diisocyanate Chemistry. *J. Nanopart. Res.* **2011**, *13*, 4829–4837.
157. Long, D.; Li, W.; Qiao, W.; Miyawaki, J.; Yoon, S.-H.; Mochida, I.; Ling, L. Graphitization Behaviour of Chemically Derived Graphene Sheets. *Nanoscale* **2011**, *3*, 3652–3656.
158. Yang, S.-T.; Chang, Y.; Wang, H.; Liu, G.; Chen, S.; Wang, Y.; Liu, Y.; Cao, A. Folding/Aggregation of Graphene Oxide and Its Application in Cu^{2+} Removal. *J. Colloid Interface Sci.* **2010**, *351*, 122–7.
159. He, F.; Fan, J.; Ma, D.; Zhang, L.; Leung, C.; Chan, H. L. The Attachment of Fe_3O_4 Nanoparticles to Graphene Oxide by Covalent Bonding. *Carbon* **2010**, *48*, 3139–3144.
160. Satti, A.; Larpent, P.; Gun'ko, Y. Improvement of Mechanical Properties of Graphene Oxide/Poly(allylamine) Composites by Chemical Crosslinking. *Carbon* **2010**, *48*, 3376–3381.
161. Liu, F.; Choi, J. Y.; Seo, T. S. Graphene Oxide Arrays for Detecting Specific DNA Hybridization by Fluorescence Resonance Energy Transfer. *Biosens. Bioelectron.* **2010**, *25*, 2361–2365.
162. Whitby, R. L. D.; Korobeinyk, A. V.; Gun'ko, V. M.; Wright, D. B.; Dichello, G.; Smith, L. C.; Fukuda, T.; Maekawa, T.; Thorpe, J. R.; Mikhalovsky, S. V. Single-Layer Graphenes Functionalized with Polyurea: Architectural Control and Biomolecule Reactivity. *J. Phys. Chem. C* **2013**, *117*, 11829–11836.
163. Kim, H.; Miura, Y.; Macosko, C. W. Graphene/Polyurethane Nanocomposites for Improved Gas Barrier and Electrical Conductivity. *Chem. Mater.* **2010**, *22*, 3441–3450.
164. Stankovich, S.; Piner, R. D.; Nguyen, S. T.; Ruoff, R. S. Synthesis and Exfoliation of Isocyanate-Treated Graphene Oxide Nanoplatelets. *Carbon* **2006**, *44*, 3342–3347.
165. Wang, J.; Wang, Y.; He, D.; Liu, Z.; Wu, H.; Wang, H.; Zhao, Y.; Zhang, H.; Yang, B. Composition and Annealing Effects in Solution-Processable Functionalized Graphene Oxide/P3ht Based Solar Cells. *Synth. Met.* **2010**, *160*, 2494–2500.
166. Zhang, D.-D.; Zu, S.-Z.; Han, B.-H. Inorganic-Organic Hybrid Porous Materials Based on Graphite Oxide Sheets. *Carbon* **2009**, *47*, 2993–3000.
167. Gomez-Navarro, C.; Meyer, J. C.; Sundaram, R. S.; Chuvilin, A.; Kurasch, S.; Burghard, M.; Kern, K.; Kaiser, U. Atomic Structure of Reduced Graphene Oxide. *Nano Lett.* **2010**, *10*, 1144–1148.
168. Guo, F.; Kim, F.; Han, T. H.; Shenoy, V. B.; Huang, J.; Hurt, R. H. Hydration-Responsive Folding and Unfolding in Graphene Oxide Liquid Crystal Phases. *ACS Nano* **2011**, *5*, 8019–8025.
169. Biju, V. Chemical Modifications and Bioconjugate Reactions of Nanomaterials for Sensing, Imaging, Drug Delivery and Therapy. *Chem. Soc. Rev.* **2014**, *43*, 744–764.
170. Tang, Z.; Shen, S.; Zhuang, J.; Wang, X. Noble-Metal-Promoted Three-Dimensional Macroassembly of Single-Layered Graphene Oxide. *Angew. Chem., Int. Ed.* **2010**, *49*, 4603–4607.
171. Paek, S.-M.; Yoo, E.; Honma, I. Enhanced Cyclic Performance and Lithium Storage Capacity of SnO_2/Graphene Nanoporous Electrodes with Three-Dimensionally Delaminated Flexible Structure. *Nano Lett.* **2009**, *9*, 72–75.
172. Williams, G.; Seger, B.; Kamat, P. V. Tio2-Graphene Nanocomposites. Uv-Assisted Photocatalytic Reduction of Graphene Oxide. *ACS Nano* **2008**, *2*, 1487–1491.
173. Xu, C.; Wang, X.; Zhu, J. Graphene-Metal Particle Nanocomposites. *J. Phys. Chem. C* **2008**, *112*, 19841–19845.
174. Liang, Y.; Li, Y.; Wang, H.; Zhou, J.; Wang, J.; Regier, T.; Dai, H. Co_3O_4 Nanocrystals on Graphene as a Synergistic Catalyst for Oxygen Reduction Reaction. *Nat. Mater.* **2011**, *10*, 780–786.
175. Mohanty, N.; Berry, V. Graphene-Based Single-Bacterium Resolution Biodevice and DNA Transistor: Interfacing Graphene Derivatives with Nanoscale and Microscale Biocomponents. *Nano Lett.* **2008**, *8*, 4469–4476.
176. Muszynski, R.; Seger, B.; Kamat, P. V. Decorating Graphene Sheets with Gold Nanoparticles. *J. Phys. Chem. C* **2008**, *112*, 5263–5266.
177. Baker, S. N.; Baker, G. A. Luminescent Carbon Nanodots: Emergent Nanolights. *Angew. Chem., Int. Ed.* **2010**, *49*, 6726–6744.
178. Shornikova, O. N.; Kogan, E. V.; Sorokina, N. E.; Avdeev, V. V. The Specific Surface Area and Porous Structure of Graphite Materials. *Russian J. Phys. Chem. A* **2009**, *83*, 1022–1025.
179. Zhang, L.; Chen, G.; Hedhili, M. N.; Zhang, H.; Wang, P. Three-Dimensional Assemblies of Graphene Prepared by a Novel Chemical Reduction-Induced Self-Assembly Method. *Nanoscale* **2012**, *4*, 7038–7045.
180. Stankovich, S.; Piner, R. D.; Chen, X. Q.; Wu, N. Q.; Nguyen, S. T.; Ruoff, R. S. Stable Aqueous Dispersions of Graphitic Nanoplatelets *via* the Reduction of Exfoliated Graphite Oxide in the Presence of Poly(sodium 4-styrenesulfonate). *J. Mater. Chem.* **2006**, *16*, 155–158.
181. Liu, H.; Gao, J.; Xue, M. Q.; Zhu, N.; Zhang, M. N.; Cao, T. B. Processing of Graphene for Electrochemical Application: Noncovalently Functionalize Graphene Sheets with Water-Soluble Electroactive Methylene Green. *Langmuir* **2009**, *25*, 12006–12010.
182. Sun, H.; Xu, Z.; Gao, C. Multifunctional, Ultra-Flyweight, Synergistically Assembled Carbon Aerogels. *Adv. Mater.* **2013**, *25*, 2554–2560.

183. Bi, H.; Xie, X.; Yin, K.; Zhou, Y.; Wan, S.; He, L.; Xu, F.; Banhart, F.; Sun, L.; Ruoff, R. S. Spongy Graphene as a Highly Efficient and Recyclable Sorbent for Oils and Organic Solvents. *Adv. Funct. Mater.* **2012**, *22*, 4421–4425.
184. Xiao, J.; Mei, D.; Li, X.; Xu, W.; Wang, D.; Graff, G. L.; Bennett, W. D.; Nie, Z.; Saraf, L. V.; Aksay, I. A.; Liu, J.; Zhang, J.-G. Hierarchically Porous Graphene as a Lithium-Air Battery Electrode. *Nano Lett.* **2011**, *11*, 5071–5078.
185. Sun, Y.; Wu, Q.; Shi, G. Supercapacitors Based on Self-Assembled Graphene Organogel. *Phys. Chem. Chem. Phys.* **2011**, *13*, 17249–17254.
186. Lee, J. S.; Ahn, H. J.; Yoon, J. C.; Jang, J. H. Three-Dimensional Nano-Foam of Few-Layer Graphene Grown by CVD for DSSC. *Phys. Chem. Chem. Phys.* **2012**, *14*, 7938–7943.
187. Yavari, F.; Chen, Z.; Thomas, A. V.; Ren, W.; Cheng, H.-M.; Koratkar, N. High Sensitivity Gas Detection Using a Macroscopic Three-Dimensional Graphene Foam Network. *Sci. Rep.* **2011**, *1*.
188. Goncalves, G. A. B.; Pires, S. M. G.; Simoes, M. M. Q.; Neves, M.; Marques, P. Three-Dimensional Graphene Oxide: A Promising Green and Sustainable Catalyst for Oxidation Reactions at Room Temperature. *Chem. Commun.* **2014**, *50*, 7673–7676.